SEDIMENTOLOGY the journal of the International Association of Sedimentologists

Sedimentology (2021) **68**, 2523–2562 doi: 10.1111/sed.12866

Coarse-grained deltas approaching shallow-water canyon heads: A case study from the Lower Pleistocene Messina Strait, Southern Italy

SERGIO G. LONGHITANO*, DOMENICO CHIARELLA†, MARCELLO GUGLIOTTA‡,§ and DARIO VENTRA¶,**

**Department of Sciences, University of Basilicata, Viale dell'Ateneo lucano, 10, Potenza, 85100, Italy*
†Clastic Sedimentology Investigation (CSI), Department of Earth Sciences, Royal Holloway University of London, Egham, Surrey, London, TW20 0EX, UK (E-mail: sergio.longhitano@unibas.it)
‡Faculty of Geosciences, University of Bremen, Klagenfurter Straße 2–4, Bremen, 28359, Germany
§MARUM – Center for Marine Environmental Sciences, University of Bremen, Leobener Straße 8, Bremen, 28359, Germany
¶Department of Earth and Environmental Science, University of Geneva, Rue des Maraîchers 13, Geneva, 1205, Switzerland
***Faculty of Geosciences, Utrecht University, Princetonlaan 8a, Utrecht, 3584 CB, The Netherlands*

Associate Editor – Christopher Fielding

ABSTRACT

The tide-dominated Messina Strait (southern Italy) is a 3 km wide marine passageway, whose block-faulted borders form steep subaqueous zones incised by canyons and gullies. These erosional features retreat towards the shorelines and are often in direct connection with subaerial valley-bounded river deltas. High-energy density-flows generated by river floods periodically enter the canyon heads, attaining supercritical-flow regime and accreting large, upslope-migrating bedforms. Although these bedforms have been documented in recent studies, little attention has been paid to the definition of the type of delta entering canyon heads, the internal features of river-influenced deposits accumulated in the nearshore zone, and their interplay with tidal currents flowing axially to the strait. This study focuses on a Lower Pleistocene coarse-grained succession exposed along the north-eastern margin of the modern Messina Strait, investigated using conventional facies analysis and sedimentological logging, integrated with photogrammetric techniques and interpretation of drone-acquired imagery. Facies confinement between basement blocks suggests a subaqueous delta complex shed from the tectonically controlled margin of the ancient strait and entering shallowly submerged canyon heads. Basal breccias, conglomerates and pebbly sandstones exhibiting channel-form discontinuities and upslope dipping backsets are interpreted as cyclic-step and antidune deposits. Units composed of these facies are comprised between master erosional surfaces and tidal ravinement surfaces. The tidal ravinements suggest that canyon infill occurred during a major phase of sea-level rise, punctuated by minor falls and stillstands. These surfaces are overlain by mixed bioclastic–siliciclastic, arenitic, trough and planar cross-strata, representing dunes migrating roughly parallel to the palaeo-coastline and originated by tidal currents amplified by the narrowing of the ancient Messina Strait. Tidal-influenced sedimentation dominated over the fluvial-influenced processes during the late transgression, overfilling the canyon relief. The exceptionally good exposure of depositional architectures and facies characteristics is key to outline

the general features of a specific type of delta system, fed by valley-bounded rivers and entering canyon heads in the nearshore of tectonically-controlled, tide-influenced steep strait margins. The pre-existing subaqueous incised topography forced the delta front to be split into lobe branches during the canyon infilling, hampering clinoform architectures and preserving large supercritical-flow sedimentary structures. This study suggests these as possible criteria for the recognition of similar systems in outcrop or subsurface.

Keywords Canyon-head deltas, cyclic steps and antidunes, Lower Pleistocene, Messina Strait, tidal dunes, tidal strait.

INTRODUCTION

The tide-dominated modern Messina Strait divides Sicily from the Italian Peninsula in the central Mediterranean (Fig. 1A) and is bordered by normal faults (Fig. 1B). This structural setting affects the morphology of the sublittoral zones, which consist of 4° to 5° dipping slopes, descending towards the deeper strait to a depth of *ca* 300 m within a distance of 1 km from the shoreline (Chiocci *et al.,* 2008). The sublittoral strait margins are incised by gullies and canyons (Fig. 1B), many of which are in continuity with their respective onshore river deltas (Chiocci & Casalbore, 2017). The rivers are bounded by valleys and form small and/or ephemeral 'river deltas' (*sensu* Nemec, 1990) typically characterized by coarse-grained sediment. The depositional activity in these deltas is mainly associated with episodic discharges resulting from intense and localized rainfall occurring after periods of dryness (e.g. Sorriso-Valvo, 2008; Casalbore *et al.,* 2011). In rare cases, these events result in catastrophic floods that cause serious damage and casualties among the local communities (for example, south-western Messina Strait, October 2009).

River deltas represent one of the major sediment sources in modern, tectonically active, highland-bordered coastal settings, including tide-dominated straits (for example, Messina, Juan de Fuca, Taiwan; Gelfenbaum *et al.,* 2015; Hsiung & Saito, 2017; Longhitano, 2018a). Marginal active faulting, mass-wasting processes and diffuse scouring phenomena are common to deltas entering tectonically active straits bordered by highly unstable subaqueous margins (Chiocci *et al.,* 2008; Longhitano & Steel, 2016; Longhitano, 2018a,b; Chiarella *et al.,* 2020). The high-relief basement setting commonly prevents these steep-fronted deltas from developing a subaerial plain, given the lack of areal accommodation (Nemec, 1990). One of the most evident features observed along the subaqueous margins of modern straits are incipient canyons (e.g. Mitchell *et al.,* 2007; Mountjoy *et al.,* 2009) which consist of shallow-marine, shelf-indenting incisions or 'shelf valleys' (*cf.* Shepard, 1981), showing either simple or multi-tributary channel patterns (e.g. Gamberi *et al.,* 2017; Gamberi, 2020).

In the modern Messina Strait (Fig. 2A), canyon heads erosionally recede close to the shore, enhancing processes of beach erosion, coastal instability and sediment bypass. Canyons promote sediment transfer to the deep basin and contribute to the scarce development of a subaerial plain (Fig. 2B to D; Cocco *et al.,* 1988; Casalbore *et al.,* 2014, 2019). Modern canyon heads correspond to river valleys in the emerged coastal areas, as they reflect the expression of ancient incised valleys transgressed after the Last Glacial Maximum (e.g. Baztan *et al.,* 2005). Consequently, modern river deltas may prograde directly into canyon heads, leading to the accumulation and preservation of thick sedimentary successions due to local accommodation and lateral confinement (Fig. 2E) that inhibit reworking by tidal surficial waves (e.g. Gamberi *et al.,* 2017; Maier *et al.,* 2018; Silva *et al.,* 2019). This condition represents a prerequisite to record the signature of high-energy, river-dominated flash floods in marine settings, whose sedimentary signatures are thought to have scarce preservation potential in shallow water compared with deep-marine settings, due to subsequent reworking by waves and tides (e.g. Mutti *et al.,* 1996). The documentation of supercritical-flow structures (such as antidunes and cyclic steps) associated with river-derived density currents in shallow-marine settings (Fig. 2B, D and E), is indeed limited to few case studies of ancient deposits (e.g. Postma, 1984; Postma & Roep, 1985; Nemec, 1990; Massari, 1996; Ventra *et al.,* 2015; Massari, 2017). However, delta to sublittoral channel heads are common along the steep margins of modern straits (e.g. Yoshikawa & Nemoto, 2010; Korup, 2012; Ortega-Sánchez

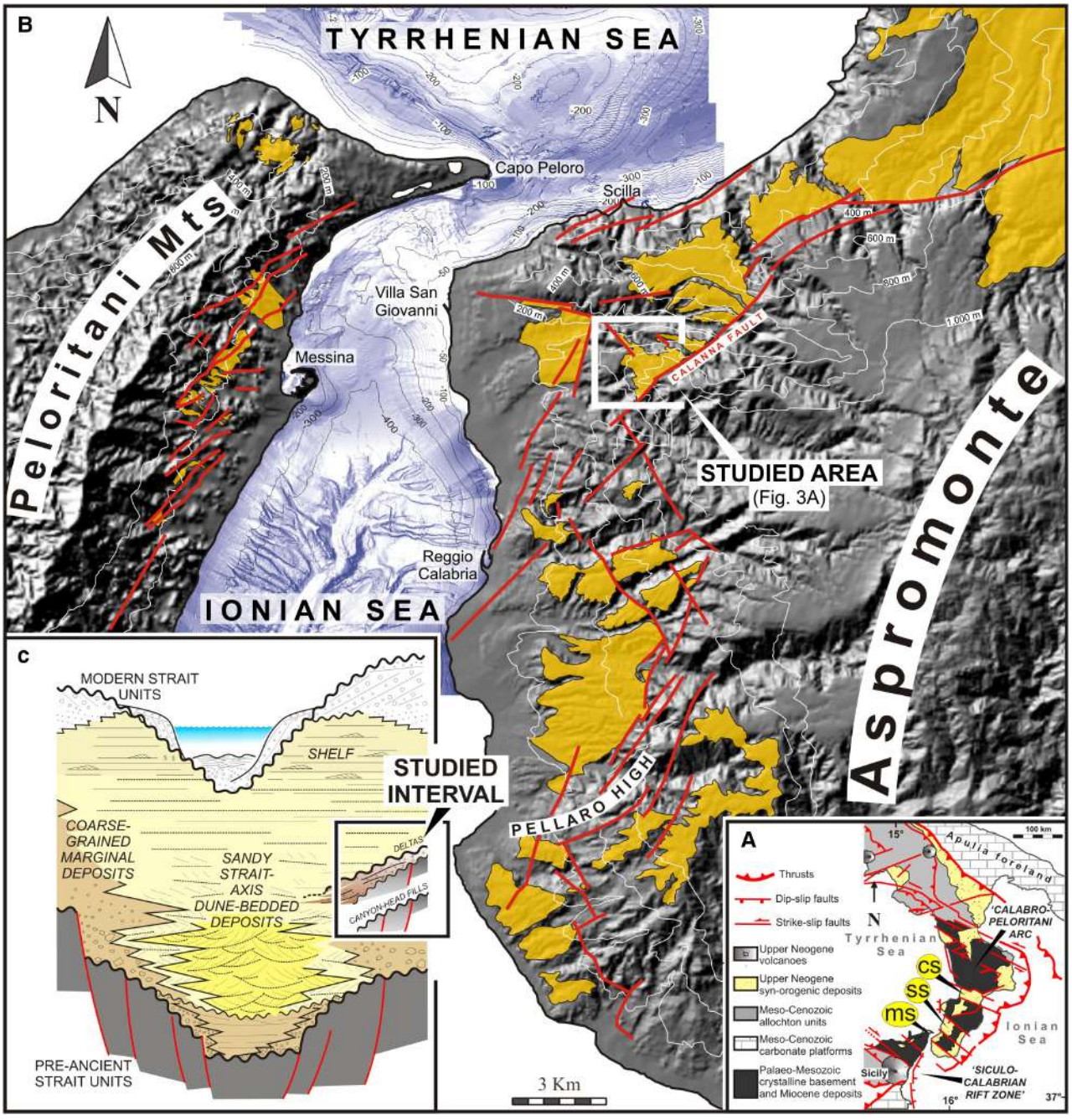

Fig. 1. (A) Structural map of southern Italy, with an indication of the main semi-regional strike-slip zones dissecting the Calabrian Arc and responsible for the shaping of the various tidal straits during the Plio-Quaternary (cs = Catanzaro Strait; ss = Siderno Strait; ms = Messina Strait). (B) Digital terrain model of north-eastern Sicily and south-western Calabria forming the onshore margins of the modern Messina Strait; the distribution of Lower Pleistocene deposits is indicated in yellow and the main Plio-Quaternary faults are represented with red lines (modified from Ghisetti *et al.*,1983). (C) East–west oriented schematic representation of the lithostratigraphy of the Messina Strait and its two margins, showing the main types of Early Pleistocene depositional environments from strait margin to the centre (modified, after Longhitano, 2018b). The box shows the approximate stratigraphic and palaeoenvironmental range inferred for the succession discussed here.

et al., 2014) and could have occurred in past systems more frequently than previously envisaged. Arguably, these types of deltas depart from conventional depositional models and need to be further identified, possibly combining observations of modern examples with ancient outcrop analogues.

This paper presents an outcrop-based study of a Lower Pleistocene succession exposed along the north-eastern margin of the modern Messina

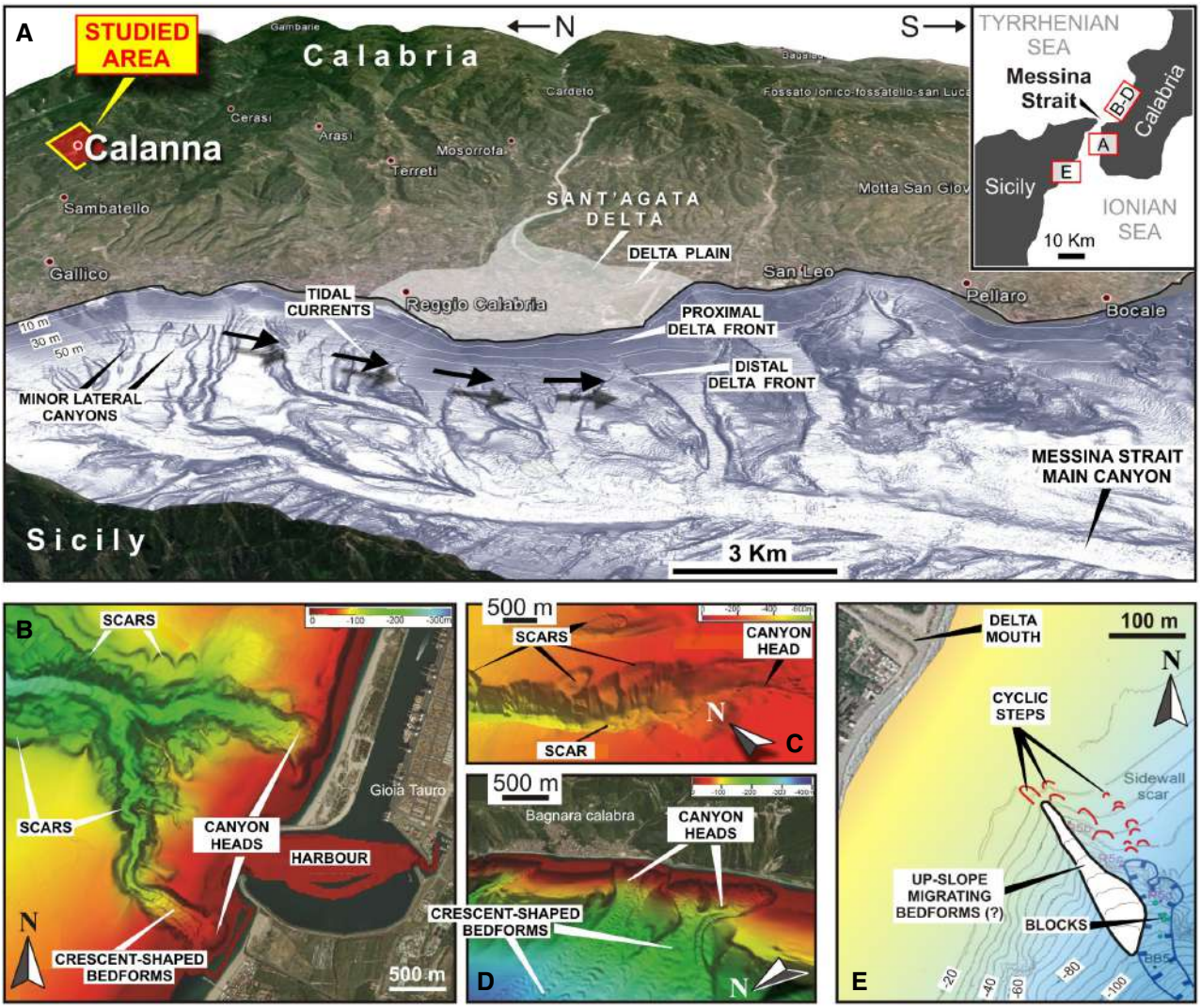

Fig. 2. Examples of depositional settings from the modern Messina Strait (see inset for locations). (A) View of the eastern margin (Calabrian) near the southern exit of the strait, with multibeam-based reconstruction of the strait bottom. The Sant'Agata River Delta is an example of present-day delta entering the strait from the margin. A number of minor canyons incise the distal delta front, which is possibly influenced by ebb tidal currents (black arrows) flowing parallel to the strait coastline. Note location of the study area on the Calabrian margin. (B) Shallow-water canyon heads indenting the sublittoral zone along the north-eastern border of the strait, near Gioia Tauro. (C) Side view of the Mesima Canyon showing multiple scars along the canyon walls. (D) Canyon heads offshore Bagnara Calabra showing internal up-slope migrating bedforms. Note connections with onshore rivers. (E) Nearshore subaqueous canyon along the south-western portion of the strait documented after the high-magnitude, flash flood event occurred on 1 October 2009. Scouring features and up-slope migrating bedforms resulted from supercritical flows violently entering the basin in the course of few hours after an intense and localized rainfall [the satellite image in (A) is from Google Earth©; multibeam data in (A) are modified, after Chiocci *et al.,*2008; images in (B), (C) and (D) are modified, after Casalbore *et al.,*2019; bathymetric data in (E) are modified, after Casalbore *et al.,*2011).

Strait (southern Italy; Figs 1B and 2A). The studied deposits located near the village of Calanna (Figs 2A and 3A to E) were investigated by means of facies analysis and sedimentological logging integrated with drone-acquired aerial photograph interpretation. The article aims to: (i) provide a sedimentary facies and architectural description of the Calanna successions; (ii) interpret such deposits as a stratigraphic signature of the subaqueous portion of a strait-margin delta complex encroaching a series of canyon heads, indenting the flank of the ancient tidal strait (Fig. 1C); and (iii) discuss a conceptual and process framework to pinpoint distinctive criteria for the recognition of canyon-head delta systems from similar successions in the rock record.

THE MODERN MESSINA STRAIT AND ITS ANCIENT ANALOGUE

The modern Messina Strait experiences semidiurnal tidal phase reversals every six hours between the Tyrrhenian and the Ionian seas (Vercelli, 1925; Defant, 1940, 1961; Bignami & Salusti, 1990; Mosetti, 1992; Lozano & Candela, 1995; Androsov *et al.,* 2002). Near the narrowest (3 km wide) and shallowest (80 m deep) strait-centre zone, tidal currents are amplified with collinear flood and ebb flows reaching 3 m sec^{-1} (Bignami & Salusti, 1990). After their transit through the most reduced hydraulic cross-section of the strait, tidal currents decelerate towards the north and the south, where the strait widens. This leads to the accumulation of fields of actively migrating sand dunes (Fig. 1B and C; Selli *et al.,* 1978; Montenat *et al.,* 1987; Santoro *et al.,* 2004; Chiocci *et al.,* 2008) that gradually become smaller down-current and interfinger with shelf mudstones further basinward, near the two opposite strait-end zones (Longhitano, 2013, 2018a). Towards the strait margins, tidal-current velocities are reduced by bottom friction, having little or no influence on sediment transport at the shoreline. Consequently, valley-bounded river deltas prograding into the strait from the sides receive little or no influence from the tidal circulation dominating the strait axis. Recent observations suggest that the dominant process regime in the sublittoral zone of the strait derives from a combination of river-derived, gravity-driven event flows, related to occasional river floods and gradient-dependent instability of the margins (e.g. Casalbore *et al.,* 2017, 2018, 2019).

The modern Messina Strait lies near the subduction zone separating the African and European plates (Malinverno & Ryan, 1986; Patacca *et al.,* 1990; Doglioni, 1991; Doglioni *et al.,* 2001; Fig. 1A). The tectonically-controlled strait dissects the top of the south-east-migrating Calabro–Peloritani Orogen, separating the back-arc Tyrrhenian Basin to the north-west and the fore-arc Ionian Basin to the south-east (Fig. 1A; Ghisetti, 1981a; Ghisetti & Vezzani, 1982; Dewey *et al.,* 1989; Lentini *et al.,* 1994; Finetti *et al.,* 1996). This regional setting leads to a complex geological history for this area, which experienced sea-strait conditions at least twice during the last 3 Myr.

A first Late Pliocene–Early Pleistocene phase of uplift, caused by an episode of contractional–transpressive deformation of the Calabro–Peloritani Orogen (de Jonge *et al.,* 1994; Monaco *et al.,* 1996), formed of a series of grabens which dissected the orogen from north to south. After a stage of relative sea-level fall, many of these basins were inundated during a subsequent Early Pleistocene marine transgression, turning into marine straits (i.e. the Catanzaro, Siderno and Messina straits in Fig. 1A). These conduits promoted exchanges of water masses and phenomena of tidal amplification with consequent accumulation of distinctive tidal facies associations (Colella & D'Alessandro, 1988; Barrier *et al.,* 1993; Longhitano *et al.,* 2012b, 2014; Longhitano, 2018a,b) analogue to those documented today in the modern Messina Strait (Selli *et al.,* 1978; Chiocci *et al.,* 2008; Fig. 1C). At the beginning of the Middle Pleistocene, a new event of regional-scale uplift led to the closure of many of these straits (e.g. Longhitano, 2012; Longhitano *et al.,* 2012b, 2014, 2020). The ancient Messina Strait was the southernmost in the system of multiple straits that connected the Tyrrhenian Basin to the north/north-west to the Ionian Basin to the east/south-east (Longhitano, 2013). Starting from the Middle Pleistocene onward, the western and eastern margins of the Messina Strait were affected by differential uplift rates, causing a diverse exposure of the Plio-Pleistocene strata between the Sicilian and the Calabrian onshore sides of the modern strait (Dumas *et al.,* 1982; Ghisetti, 1984; Westaway, 1993; Monaco *et al.,* 1996; Fig. 1B). The resulting outcrops preserve strait-marginal and sublittoral deposits (e.g. Chiarella *et al.,* 2020), whereas the corresponding strait-axial sediments

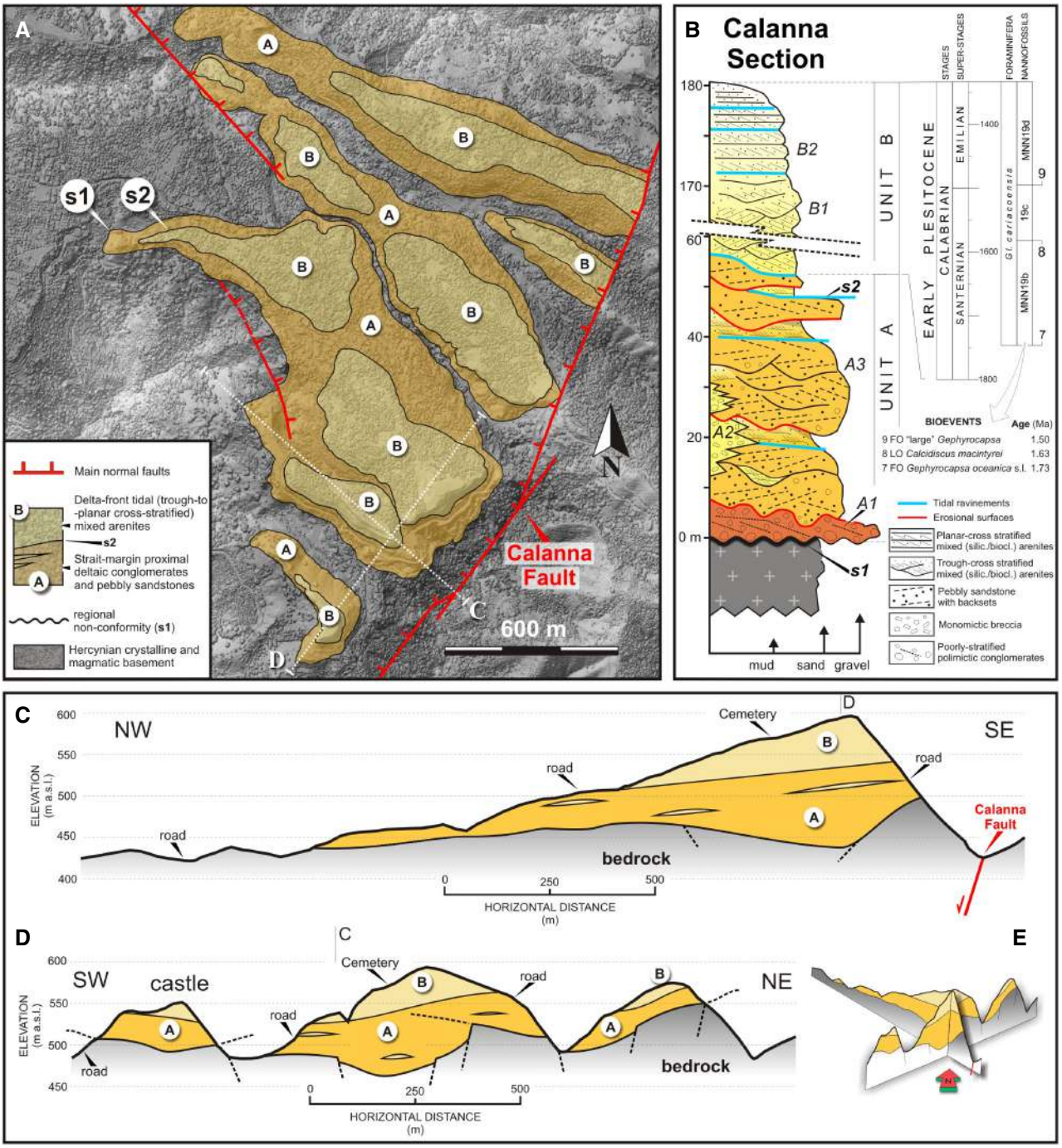

Fig. 3. (A) Digital terrain model (DTM)-based geological map of the study area, with plan-view distribution of the Lower Pleistocene succession. (B) Stratigraphic column of the sedimentary succession exposed near Calanna, including the two main lithostratigraphic units *A* and *B* (biostratigraphic data are from Longhitano *et al.,* 2012b). s1 and s2 represent the master discontinuities. (C) and (D) Geological cross-sections reconstructed from the map in (A). (E) Oriented, 3D perspective of the two cross-sections.

currently lie beneath the modern strait bottom, sealed by Holocene marine sediments (Longhitano, 2018b; Fig. 1C).

The tide-dominated stage of the ancient Messina Strait (Barrier, 1986, 1987a,b) is recorded in the Lower Pleistocene interval, comprised

between the base of the Gelasian (*ca* 2.5 Ma) and the Calabrian (Santernian, *ca* 1.5 Ma; Barrier, 1984; Barrier *et al.,* 1987; Mercier *et al.,* 1987; Stefano & Longhitano, 2009; Longhitano *et al.,* 2012b). This interval includes a number of facies associations (Fig. 1C) reflecting specific depositional zones of the ancient strait, which were interpreted based on the correspondence with the modern geomorphic and bathymetric setting (Longhitano, 2018b). These 200 m thick tidal deposits (Fig. 1B) provide excellent sedimentary records for the reconstruction of the depositional setting of discrete parts of the ancient Messina Strait (Longhitano, 2018a,b), including its borders and associated strait-marginal facies.

The Calanna section

One of the most outstanding outcrops of Pleistocene deposits of the eastern onshore border of the Messina Strait is exposed between 380 m and 580 m above sea level (a.s.l.) near the village of Calanna, in the north-eastern onshore of the modern strait (Figs 1B, 2A and 3A). The succession non-conformably laps onto the block-faulted Hercynian magmatic basement (Fig. 3A and C to E) and has been interpreted as the result of the accumulation of mass-wasting processes descending from the north-eastern, tectonically active margin of the ancient Messina Strait during the Early Pleistocene (Barrier *et al.,* 1987; Mercier *et al.,* 1987; Longhitano *et al.,* 2012b; Longhitano, 2018b). The recent uplift and consequent subaerial exposure have sculpted these deposits into a series of elongated ridges dipping towards the west/north-west (Fig. 3A), where differently oriented cliffs provide a three-dimensional exposure of a sedimentary succession *ca* 150 to 200 m thick (Fig. 3B). When reconstructed in two-dimensional cross-sections (Fig. 3C and D), strata show lateral variability in thickness, possibly due to pre-existent topographic lows striking NNW-ward (Fig. 3E). Two main cliffs (Fig. 4A to C) represent the focus of this study and consist of well-preserved exposures that can be observed both at a distance, gaining general architectural information, and that are also directly accessible for detailed facies analysis along road cuts (Fig. 4B and C).

The studied sedimentary succession is bounded south-eastward by a north-east/south-west-oriented normal fault array, known as the 'Calanna Fault' (Figs 1B, 3A and 4A), which has presumably been active since the Middle Pleistocene (Ghisetti, 1981a,b; 1984) playing an important role in steepening the sublittoral area of this part of the Messina Strait during the accumulation of the studied deposits. The Calanna sections are exposed in two main cliffs oriented parallel and perpendicular to the Calanna Fault (Fig. 4A). The perpendicular cliff strikes from south-east to north-west, approximately along the depositional dip, and provides an outcrop exposure of *ca* 640 m in length and *ca* 200 m in height (Fig. 4B). The parallel cliff is oriented from south-west to north-east, exposing an outcrop of *ca* 390 m in length and less than 100 m in height, oriented roughly along-strike (Fig. 4C). Both sections reveal two vertically stacked stratal units *A* and *B*, which have been distinguished based on their facies and architectural characters (Figs 4B, 4C and 5A).

METHODOLOGY

The dataset derives from the field-based study of the Calanna succession (Fig. 4A to C), which has been investigated by facies analysis, sedimentological logging techniques and aerial collected photographs. The descriptive terminology follows Harms *et al.* (1975, 1982) and Collinson & Mountney (2006). Sedimentary facies were distinguished based on their macroscopic characteristics (Harms *et al.,* 1982; Walker, 1984), including bed thickness, lithology, clast composition, grain size, sedimentary structures, and trace-fossil and body-fossil assemblages. Terminology for gravel-sized clasts follows the Blair & McPherson (1999) textural classification for coarse-grained sediments. Since a considerable volume of the investigated deposits are arenites of mixed composition, henceforth called 'bioclastic–siliciclastic arenites', the 'bioclastic/siliciclastic ratio' (b/s) and the 'Segregation Index' (S.I. *cf.* Chiarella & Longhitano, 2012) were estimated for each facies, in order to quantify the percentage of the dominant clastic component and the degree of separation between siliciclastic and bioclastic particles. The Bioturbation Index (B.I.), quantifying the relative (percent) volume of sediment affected by bioturbation has been applied following Taylor & Goldring (1993), together with the ichnofacies identification criteria following Minter*et al.* (2016). Large-scale depositional architectures were constrained using photomosaics and three-dimensional outcrop models obtained from the integration of LIght Detection And Ranging

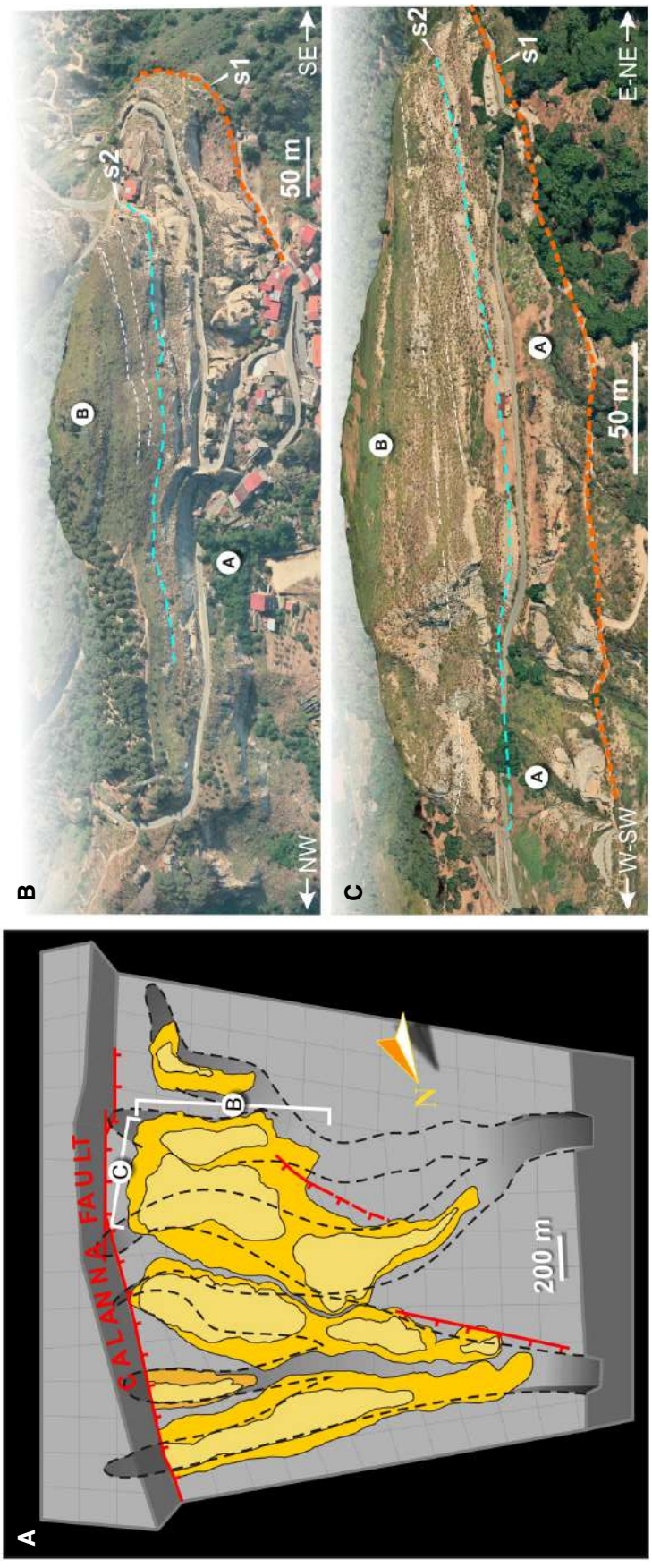

Fig. 4. (A) Block-diagram showing the geometric relationship between the studied outcrop deposits (yellow) and the Calanna Fault. Deposits occupy the hanging-wall block of the fault zone, which is suggested to represent the strait-margin sublittoral sector during the Early Pleistocene. Dashed black lines indicate possible canyons incising the slope prior to deposition. The succession is exposed three-dimensionally along two main cliffs (B) and (C). Here, the dashed red line (s1) indicates the base of the succession, corresponding with a non-conformity surface, whereas the dashed blue line (s2) is the discontinuity separating the underlying Unit *A* from the overlying Unit *B*.

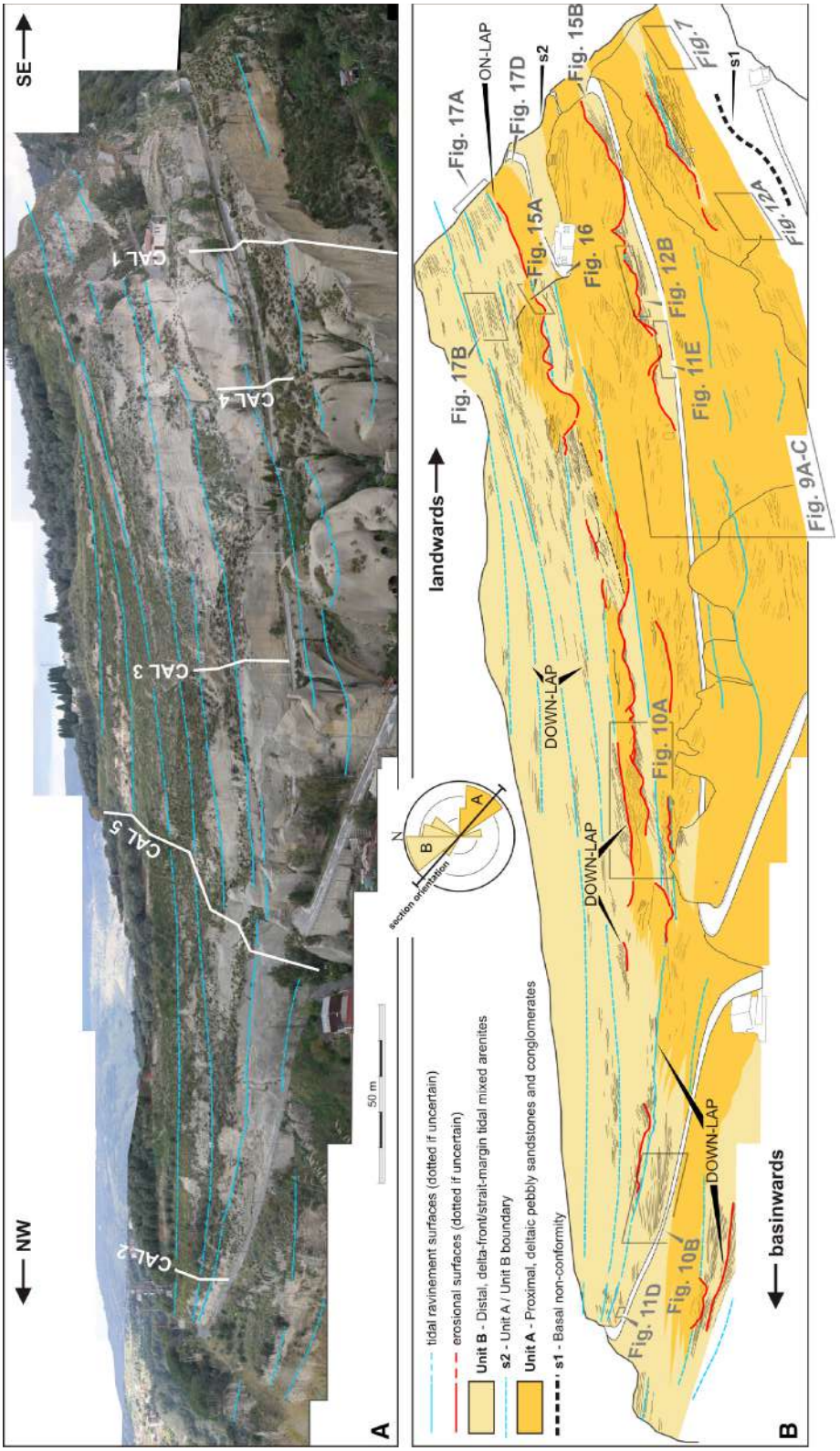

Fig. 5. (A) Photomosaic of a panoramic view of the Calanna north-west/south-east oriented cliff (see Fig. 3); white lines indicate the position and vertical extent of the sedimentological logs (Fig. 6). (B) Line-drawing of the section highlighting the lateral–vertical extent of the two units *A* and *B*. Some major architectural elements are traced and the locations of the main outcrop photographs are indicated.

(LIDAR) scanning, drone flights and Digital Terrain Models (DTM). Palaeocurrents were measured from pebble imbrication and foreset dip values of cross-bedding and plotted on stereonet diagrams, aiming at reconstructing the main direction of accretion of sand bodies.

RESULTS

Litho-stratigraphy and large-scale depositional architectures

The succession exposed near the village of Calanna consists of two litho-stratigraphic units (*A* and *B*) for a total thickness of 185 m. The succession exhibits two groups of bounding master discontinuities: (i) a number of low relief and gently sloping surfaces (blue lines in Fig. 5A and B) converging towards the west/north-west (basinward) and slightly diverging in the opposite direction (landward), also due to the syn-sedimentary displacement exerted by the Calanna Fault (see Fig. 4A); (ii) erosional discontinuities (red lines in Fig. 5B), mostly in Unit *A* and matching with, or incising onto, the underlying low relief surfaces. These surfaces bound intervals, each one consisting of strata with downlapping terminations to the lower bounding surfaces. The above-described physical features are regarded as signatures of relative sea-level change and have been used in the reconstruction of a generalized sea-level curve, which will be discussed later on.

Unit A

The lower Unit *A* overlies the basement with a non-conformity surface (s1 in Fig. 5B), is up to 90 m thick in the south-east area (upslope) and thins towards the north-west (down-slope) until pinching out over a few hundreds of metres. Unit *A* consists mainly of fossiliferous pebbly sandstones with basal conglomerates and sporadic sandstone intercalations. The large-scale depositional architecture of Unit *A* is defined by the previously described low relief master surfaces and by the presence of irregular, erosional surfaces (blue and red lines in Fig. 5B, respectively). These latter are composite undulate discontinuities, forming up to 100 m long trains of shallow U-shaped scours dominantly filled by upslope-dipping backsets (Fig. 5B). Bed-sets comprised between these discontinuities range in thickness from 4 to 12 m and lap against the basement unit with a back-stepping geometry (Fig. 5B). Internally, lower-rank erosional surfaces have cross-cutting relationships and delimitate cross-strata sets with variable thickness and geometry. Cross-strata consist of angular, tangential and sigmoidal, 3 to 6 m thick sets, locally including basal breccias.

Unit B

The upper Unit *B* is up to 95 m thick and is partially interbedded with or overlies Unit *A* on a low relief surface (s2 in Fig. 5B). Sediments are mixed bioclastic–siliciclastic arenites, with rare breccia intervals and with a general thinning-upward trend for individual cross-strata. The section's large-scale architecture consists of a series of vertically stacked sedimentary bodies, westward-dipping, wedging out basinward and back-stepping onto the block-faulted substrate, separated by the low relief master surfaces described above (blue lines in Fig. 5B). Unit *B* can be subdivided into two main intervals (lower and upper) based on the vertical transition from three-dimensional to two-dimensional cross-strata (Longhitano *et al.,* 2012b, 2014). Internally, different hierarchical orders of stacked sets of trough-based and planar-based stratification occur, dipping towards north/north-west, with thicknesses of 12 to 15 m in the basinward areas thinning progressively towards the margin (south/south-east). Foresets contain a variety of internal smaller-scale structures, whose features are described in the following sections and summarized in Table 1.

Facies and facies associations

The two main stratigraphic units recognized in the studied sections (Figs 3B, 4 and 5) correspond to two main facies associations defined from the sedimentological analysis (Table 1). Facies association *A* includes basal conglomerates (*A1*), breccias (*A2*), and fossiliferous, pebbly coarse-grained sandstones and conglomerates (*A3*; Fig. 6). Facies association *B* consists of trough cross-stratified and planar-cross-stratified, coarse-grained mixed (bioclastic–siliciclastic) arenites (*B1 to B2*) intercalated with highly bioturbated, fine-grained mixed arenites (Fig. 3B).

Facies *A1* – Deltaic mouth-bar conglomerates

Description

Facies *A1* is exposed at the base of the dip-perpendicular cliff, close to its south-eastern termination. It has been documented in the *CAL 1* log

Table 1. Summary of the facies and facies associations (FA) and their quantitative features recognized in the studied succession, including the correspondent suggested genetic processes.

Stratigraphic Unit/FA	Facies	Description	Average bed thickness (m)	Bioclastic/siliciclastic ratio (b/s) (Chiarella & Longhitano, 2012)	Segregation Index (S.I.)	Bioturbation Index (B.I.) Taylor & Goldring (1993)	Fossils	Ichnofacies Minter *et al.* (2016)	Interpretation	
B	B2	*Tidal-influenced, strait-marginal, planar cross-stratified mixed arenites* Coarse to medium-sand size tabular cross-stratified mixed (siliciclastic–bioclastic) arenites	0.2–1.0	1 to >>1 (0.7–7.0)	Moderately to well segregated (>70)	Moderate to common (3–4)	Fragments of echinoids, bryozoans, gastropods, bivalves	*Thalassinoides Skolithos*	Distal delta-front two-dimensional tidal dunes forming extensive bedform fields	
	B1	*Tidal-influenced, distal delta-front, trough cross-stratified mixed arenites* Very-coarse to coarse-sand size trough cross-stratified mixed (siliciclastic–bioclastic) arenites, organized into thick erosional bed-sets, intercalated with thinner, medium-fine mixed (siliciclastic–bioclastic) deposits, heavily bioturbated	0.5–4.0	*ca* 1 (0.75–1.2)	Unsegregated to moderately segregated <35 to 50–60	Common to abundant (4–5)	Bivalves, echinoderms	*Thalassinoides*	Proximal delta-front three-dimensional tidal dunes and inter-dunes, locally filling 2–3 m deep erosional scours due to high-magnitude river-generated bypass and erosion	DEEPENING ↑
A	A3	*River-dominated, proximal delta-front pebbly sandstones* Pebbly sandstones including very-coarse sand and *ca* 15% of granules and gravel-size pebbles up to 4 cm in diameter. Scattered granitic cobble-size clasts up to 25 cm in diameter.	0.7–7.0	<<1 (0.002–0.4)	Unsegregated (30–35)	Uncommon (2)	Fragments of large-size pectinids, bryozoans and other undefined bioclasts	–	Proximal-delta supercritical-flow bedforms, including cyclic steps and antidunes, generated by local accelerations of river-generated flows entering a funnelled canyon	

Table 1. (continued)

Stratigraphic Unit/FA	Facies	Description	Average bed thickness (m)	Bioclastic/siliciclastic ratio (b/s) (Chiarella & Longhitano, 2012)	Segregation Index (S.I.)	Bioturbation Index (B.I.) Taylor & Goldring (1993)	Fossils	Ichnofacies Minter *et al.* (2016)	Interpretation
		Pebbly sandstones and conglomerates filling multi-storey scour-and-fill units, with indistinct east and south-east-dipping foresets. Parallel to low-angle-laminated or undulated 3 to 5 cm thick strata							head in the sublittoral strait-margin zone
	A2	*Basal/marginal collapse breccia* Clast to matrix-supported, monomictic angular pebble and cobble-size granitic breccia	0.5–1.7	<<1 (0.15–0.22)	Unsegregated (20)	Absent (0)	Fragments of bryozoans, and bivalves	–	Immature breccia accumulations deriving from canyon-wall collapses forming chaotic deposits in a shallow delta area swept by waves and tidal currents
	A1	*Deltaic mouth-bar conglomerates* Poorly to moderately-sorted polymictic, clast-supported conglomerates and matrix-supported gravelly very-coarse sandstones, lying erosionally on the crystalline basement. Clasts are oligomictic to polymictic very-coarse gravels and cobbles, well rounded and spherical. Sparse larger angular boulders up to 70 cm diameter	1.0–1.5	<<1 (0.15–0.22)	Unsegregated (20)	Absent (0)	Pectinids, Venus shells and other undefined bioclasts	–	Mass-transport deposits deriving from river-flooding high-density debris flows, bypassing the intertidal strait–margin zone, accumulating in a proximal and shallow delta area and forming mouth-bar conglomerates

where it is up to *ca* 3 m thick (Fig. 6) and crops out for approximately 50 m of lateral extent. Sediments of Facies *A1* (Fig. 7A) represent 5% of Unit *A* by volume and consist of poorly to moderately sorted, polymictic, clast-supported conglomerates and locally of matrix-supported, gravel-bearing, very-coarse sandstones. Clasts are well-rounded and range from large pebble to cobble in grain size, with a mode of 5 to 8 cm in diameter (Fig. 7B). Sub-angular to sub-rounded boulders up to 70 cm long also occur, in places. The majority of clasts consist of granite, but basalt, schist and sandstone lithologies are also present. Pectinid and *Venus* shell fragments are locally mixed with other bioclasts of unspecified origin, representing less than 10% of sediment by volume. Facies *A1* shows crude cross-stratification defined by abrupt grain-size changes or clast fabrics (Fig. 7C) and local sigmoidal geometry (Fig. 7D). The base of Facies *A1* is visible only locally, revealing the direct contact with the underlying crystalline basement (surface s1 in Figs 5B and 6), whereas the top is overlain by pebbly sandstones of Facies *A3* (Fig. 7A and B). The top is a highly irregular erosional surface that scours into the conglomerates with incisions up to 2 to 3 m deep (Fig. 7C).

Interpretation

The abundance of granitic basement clasts admixed with subordinate elements of different lithologies and their well-rounded shape reflects the bedrock geology of the nearby mountainous areas, and indicates that clasts were possibly recycled from pre-existing accumulations, probably including gravelly beaches along the shoreline. The presence of shell fragments suggests that the deposition of much of these sediments occurred in a shallow-water environment. Crude cross-stratification suggests rapid accretion of lithosomes, which can be indicative of mouth-bar accumulations (e.g. Mutti *et al.,* 1996; Tinterri, 2011) analogous to those developing at the front of modern coarse-grained, steep-face deposits prograding from rocky coastlines (Nemec, 1990). The overlying irregular erosional surface scouring for 2 to 3 m the deposits Facies *A1* indicates subsequent high-magnitude erosional events and sediment bypass associated with the deposition of pebbly sandstones of Facies *A3*.

In view of their stratigraphic occurrence in direct contact with an erosional surface (s1) with the basement (Fig. 8A) and of their physical attributes, the coarse-grained deposits of Facies *A1* are interpreted as the product of mass-transport processes related to subaqueous density flows, possibly generated by energetic river-discharge episodes (Orton & Reading, 1993). The relatively high maturity of clasts suggests protracted transport by rivers, whereas most of the finer sediments likely bypassed this depositional area. This is typical of hyperconcentrated flows entering shallow waters and rapidly decelerating due to bottom friction and flow expansion (Mulder & Alexander, 2001; Sohn *et al.,* 2002; Pierson, 2005; Nemec, 2009).

Facies *A2* – Basal/marginal collapse breccia

Description

Facies *A2* is observed at the base of the dip-parallel cliff (Fig. 4C), in a proximal position relative to the north-eastern termination of the outcrop. It consists of angular pebble-size and cobble-size granite clasts. These texturally immature deposits represent 3% of Unit *A* by volume and lie in direct contact with the basement rocks (Fig. 8A and B). Sediments exhibit a chaotic texture, and are often clast-supported, although a secondary matrix is locally present. A poorly-defined cross-stratification is present locally (Fig. 8C). Mollusc and bryozoan fragments have occasionally been detected (Fig. 8D). Facies *A2* is often interbedded with, or overlain by, cross-stratified mixed arenites of Facies *B1* (Fig. 8B).

Interpretation

The deposits of facies *A2* are interpreted to record episodic collapses of locally fractured and intensely faulted portions of basement cliffs or canyon walls. Rock falls may have occurred for a number of possible reasons: instability of weathered margins, earthquakes and the transit of energetic sediment-laden flows coming from more proximal areas in confined channels. The resulting accumulations thus represent subaqueous 'colluvium' (Blikra & Nemec, 1998; Millar, 2015) accumulated after minimal transport at the toe of the palaeo-cliff, and subsequently reworked in part by currents responsible for the accumulation of mixed cross-stratified intercalations. The fine-grained matrix surrounding larger clasts may derive from post-depositional infilling of openwork inter-particle spaces. Sparse remains of shells, bryozoans and encrustation by organisms typically living in the intertidal zone indicate that mass-transport processes affected bio-communities adapted to rocky substrates in a high-energy proximal setting.

Facies *A3* – River-dominated, proximal delta-front pebbly sandstones

Description

Facies *A3* crops out extensively in the lower stratigraphic interval of the strike-oriented cliff (Fig. 4B) and at the base of the dip-parallel cliff (Fig. 4C), and it has been identified in all measured logs, representing 92% of Unit *A* by volume. Facies *A3* forms a succession up to 90 m thick and reveals two main orders of bounding surfaces (Figs 5, 6 and 9A): (i) first-order surfaces are low relief, planar discontinuities, comprising 8 to 15 m thick bed-sets (blue lines in Figs 5B, 9B and 10A); (ii) second-order surfaces are cross-cutting, concave-up discontinuities internal to each bed-set and comprising multi-storey, upslope-dipping backsets with sigmoidal geometry (red lines in Fig. 9C and D) and downslope-dipping foresets (Figs 9B and 10), showing downlap stratal terminations further basinward (Fig. 10B). These structures are often associated with channelized scours filled by highly deformed strata (Fig. 10A). In strike-oriented sections, they form low-angle cross-stratification separated by slightly concave-up and convex-up discontinuities (Fig. 9E). Bed-sets of Facies *A3* consist of poorly sorted, very coarse sandstones (Fig. 11A) containing *ca* 15% of granules and spheroidal/platy pebbles up to 4 cm overlying the irregular erosional first order basal surfaces (Fig. 10A). These elements are crudely aligned, indicating cross-strata up to 1 m thick (Fig. 11A and B). Fragments of pectinids up to 3 cm large are sparsely present (Fig. 11C). Isolated, 50 to 70 cm thick lenses of granitic cobbles (up to 25 cm in diameter) derived from the basement occur locally (Fig. 11D). Bed-sets are topped by first-order, sharp low relief surfaces (blue lines in Fig. 5B), recording an abrupt transition to Facies *B1*, here represented by 0.5 to 1.2 m thick cross-stratified mixed, siliciclastic–bioclastic arenites, showing foresets dominantly migrating to the north-west (Fig. 9A and B) or exhibit 3 to 5 cm thick planar-parallel to low-angle cross-strata, forming wavy geometries (Fig. 11E). Bioclasts are more abundant here, usually up to 20% by volume, mostly deriving from fragments of pectinids and bryozoans. Multi-storey scour-and-fill structures are recurrently observable within Facies *A3* (Figs 9B, 10, 12A, 12B and 13), as well as intercalations of very coarse sands and pebbles filling local, 1 to 2 m thick, single-storey and multi-storey scours or channels (Fig. 12, inset) with soft-sediment deformation occupying the axial portion of small channels.

Interpretation

First-order low relief surfaces bounding individual bed-sets of Unit *A* and locally overlain by remnants of tidal cross-strata of Facies Association B are here interpreted to represent a type of tidal ravinement. They regularly mark the stacking pattern within Unit *A* and indicate an overall transgressive trend. This type of tidal ravinement differs from the more 'classical' tidal ravinement detected in estuarine settings (e.g. Zaitlin *et al.,* 1994), where erosion is exerted by the entrenchment of tidal channels onto underlying fluvial deposits in coastal areas as a consequence of landward migration of the zone of maximum tidal energy (e.g. Allen & Posamentier, 1993). Tidal ravinements in straits may derive from a process of lateral expansion of the tidal currents flowing parallel to the strait coastlines during major transgressions, resulting in winnowing of underlying (lowstand to early-transgressive) strait-margin systems, such as deltas or shorefaces (e.g. Longhitano, 2018b; Telesca *et al.,* 2020).

Second-order erosional irregular surfaces internal to each bed-set of Unit *A* are thought to be originated by fluvial-derived jet-flow propagation and bottom scouring upon entering the sublittoral zone. Erosion was exerted by energetic supercritical hyperpycnal flows (Russell & Arnott, 2003; Yang *et al.,* 2017; Shanmugam, 2018) transferring coarse-grained sediment from subaerial canyons to the basin. Second-order discontinuities positioned within each bed-set and forming multi-storey scour-and-fill structures may be indicative of low rates of aggradation under cyclic steps (e.g. Massari, 1996; Fielding, 2006; Alexander, 2008; Yokokawa *et al.,* 2009; Cartigny *et al.,* 2011; Lang & Winsemann, 2013; Cartigny *et al.,* 2014; Hage *et al.,* 2018). They would record dominant erosion and bypass by the highest energetic stages of the flows, rapidly followed by filling of the depressions by currents undergoing hydraulic jumps and recurrent transitions from subcritical to supercritical flow regime (Fig. 14). The process of supercritical-bedform migration was likely not continuous, but characterized by depositional episodes of dominant aggradation alternating with stages of bypass or net erosion (e.g. Cartigny *et al.,* 2014; Ventra *et al.,* 2015; Hage *et al.,* 2018; Cornard & Pickering, 2019; Kostic

et al., 2019; Stacey *et al.,* 2019; West *et al.,* 2019). The immature texture of the pebbly sandstones suggests rapid deposition of mixed bedload and suspended load under supercritical-flow conditions, as indicated by the variable number of fining-upward intervals (FU in Fig. 13) within upstream-accreting sigmoidal backsets (Fig. 9A to D). Structures at the top of the bed-sets of Unit *A* suggest that after early depositional stages, gravity flows may have evolved in two different ways:

1 Once released, the majority of the bedload flows gradually waned in energy, maintaining supercritical conditions for an amount of time sufficient to accumulate finer sandy sediments into antidune trains. This latter aggradational phase reshaped the tops of the underlying large bedforms into a relief comprising the convex profiles of smaller antidune bedforms.

2 Occasionally, the waning phase of currents was more rapid, with a transformation from supercritical into subcritical turbidity currents taking place possibly at plunge points near the shoreline (Kostic *et al.,* 2002; Lamb *et al.,* 2010), favouring the accumulation of down-current migrating dune fields.

Common to both pathways of flow evolution would be a final stage of flow halting, followed by long-term tidal reworking that led to the development of the cross-stratified intervals preserved at the top of each succession, and recording interstages of relative sea-level rises (Fig. 13).

The bioclastic content suggests that high-density fluvial outflows bypassed mouth-bar and delta-front zones, entraining living organisms (or their remains) adapted to an energetic shore environment. The occurrence of basement blocks, as well as fragments of adjacent deposits (i.e. Facies *A1* and *B1*; Fig. 8A and B), also suggests continuous scouring of the substrate in a highly energetic proximal delta-front setting, or collapses of subaqueous substrate margins.

The overall sedimentological evidence indicates a proximal subaqueous delta-front setting (Nemec, 1990; Bhattacharya, 2006). The riverine derivation of these sediment flows is inferred from the general textural immaturity of sandstones and from the presence of scattered gravel-size, well-rounded elements, which are all typical indicators of fluvial sediment discharge (e.g. Fielding, 2006). The distal wedging-out of individual bed-sets over a distance of 150 to 200 m (see Fig. 10B) may indicate that sediment fines basinward, as it is typical of proximal to distal subaqueous deltaic wedges with no relevant clinoform architectures.

Facies *B1* – Tidal-influenced, distal delta-front, trough cross-stratified mixed arenites

Description

Facies *B1* has been recognized in all measured logs (Fig. 6), forming the dominant type of deposits in Unit *B*. Facies *B1* usually overlies beds of Facies *A3* through a low relief surface (s2 in Fig. 15A) or is intercalated as remnants overlying low relief master surfaces and incised by the erosional surfaces of Facies *A3* (Figs 9B, 9D, 10 and 12B).

Sediments of Facies *B1* consist of very-coarse to coarse-grained mixed siliciclastic–bioclastic arenites with a *b/s ratio* of *ca* 1 (0.75 to 1.2), forming a compositional mixing (*sensu* Chiarella *et al.,* 2017) and organized into 0.3 to 2.0 m thick cross-strata. Their bases are erosional with a dominant concave-up geometry, whereas tops are either erosional or gradational (Fig. 15B). Cross-strata sets are locally interrupted by 10 to 15 m wide and 3 to 5 m deep scour surfaces filled by trough cross-strata (Fig. 15A and B). 'Compound' foreset architectures dominate (Fig. 16A), consisting of multiple lamina-sets superimposed over the top and the frontal (lee) side of underlying larger cross-strata (Allen, 1980; Dalrymple, 1984; Ashley, 1990; Dalrymple, 2010). Palaeocurrents derived from individual foresets mostly show a north/north-west direction, but they also include subordinate reversal indicators trending mostly to the south/south-east. Internally, reactivation surfaces (Fig. 16B) separate 10 to 30 cm thick lamina-sets of moderately to well-sorted, medium to very coarse-grained sandstones, including scattered pebbles generally <1 cm in diameter, alternating with lamina-sets made up of bioclasts (fragments of molluscs and bryozoans). Lamina-sets exhibit cyclical thickening-upward and thinning-upward bed-thickness trends associated with coarsening-upward and fining-upward grain-size repetitions (Fig. 16C). Foreset laminae show either angular or tangential geometries, often interrupted by internal discontinuities. Bioclastic–siliciclastic laminae are unsegregated to moderately segregated, indicating a *Segregation Index* (S.I.) ranging from <35 to 50–60 (*cf.* Chiarella & Longhitano, 2012). Intercalations of unsegregated (S.I. <35) siliciclastic–bioclastic sandstones, 20 to 70 cm thick, are present at

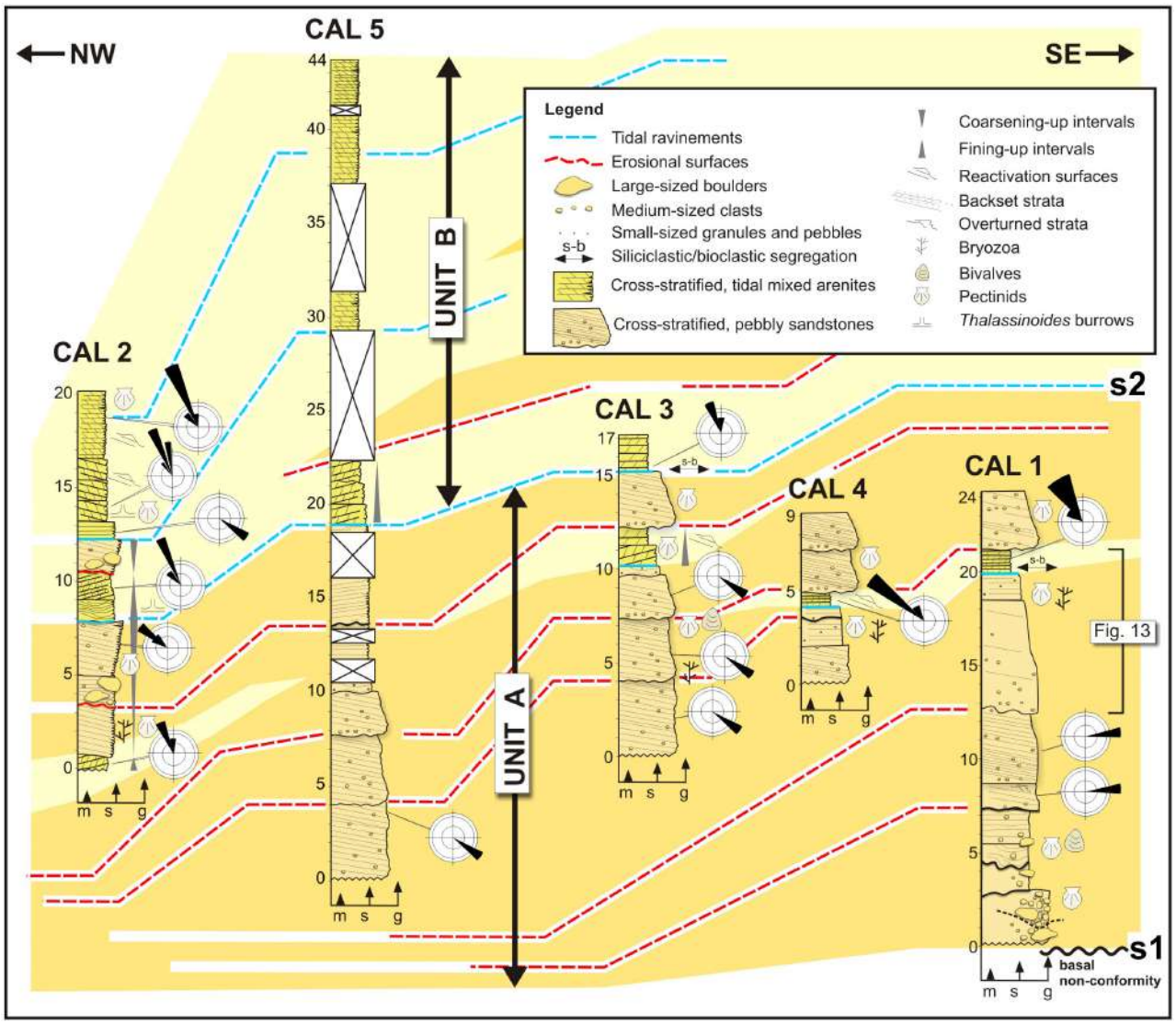

Fig. 6. Correlation panel among sedimentological logs CAL 1 to CAL 5 measured along the north-west/south-east oriented cliff of the Calanna section (see Fig. 5A for location). Palaeocurrent measurements were obtained from cross-stratification. For facies codes, refer to Table 1 (logs 1 to 4 were measured on the outcrops; log 5 was obtained from LIDAR data; s1 = base of the succession; s2 = Unit *A*/Unit *B* boundary).

various stratigraphic heights. These intervals are heavily bioturbated (B.I. 4 to 5) with *Thalassinoides* ichnofacies (Fig. 16D) that mostly obliterate primary sedimentary structures. However, planar to low-angle cross-lamination is visible in places.

Interpretation

Strata of Unit *B* stacks over the low relief discontinuity represented by surface s2 (Figs 5B, 15A and 17A), which coincides with one of the tidal ravinements recognized in the succession, indicating a phase of accelerated relative sea-level rise. The presence of bundles in the stacking pattern of cross-lamination, reactivation surfaces, alternation of angular and tangential terminations of foreset laminae, and bi-directional foreset orientations (Figs 16 and 17) suggest a tidal origin for the deposits of Facies *B1* (e.g. Allen, 1980; Homewood & Allen, 1981; Allen, 1982; Nio & Yang, 1991; Longhitano *et al.,* 2012a; Chiarella, 2016). In particular, rhythmic alternations of bioclastic and siliciclastic foreset laminae in cross-strata are thought to reproduce semi-diurnal reversal flood–ebb tidal phases in mixed systems (Longhitano, 2011), analogous to

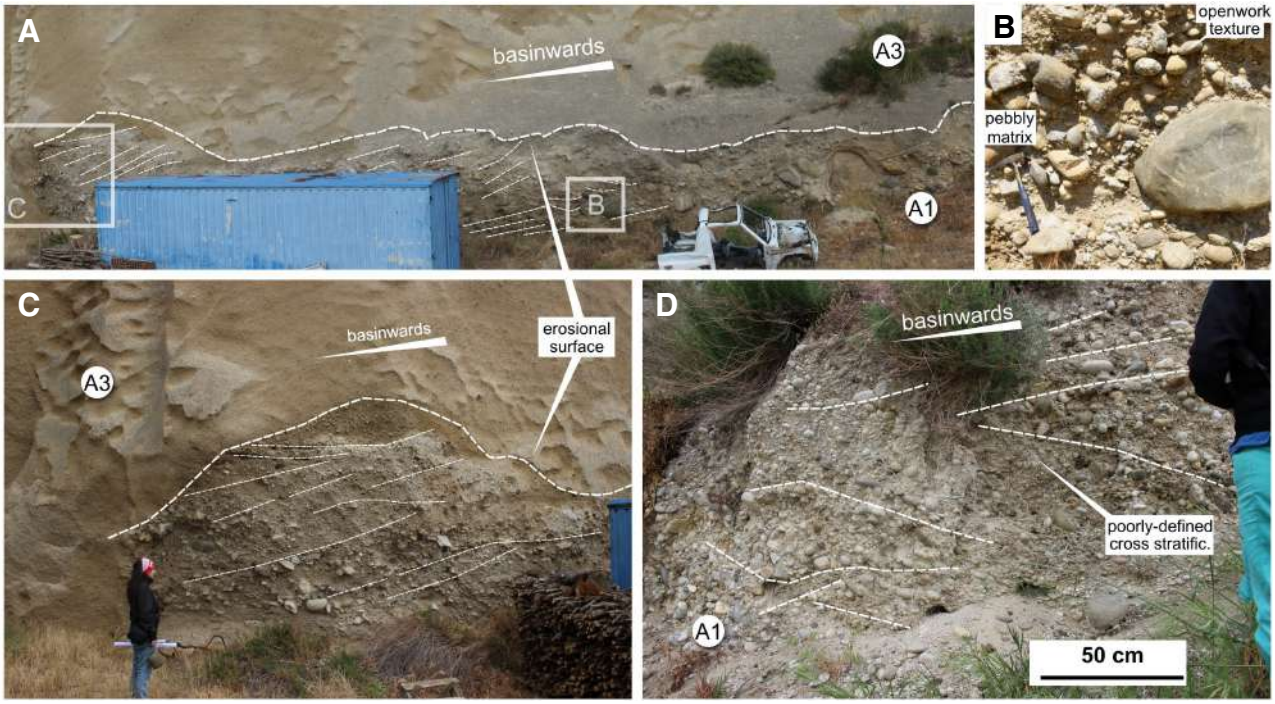

Fig. 7. Outcrop photographs of Facies *A1*, exposed at the base of the studied section (see Fig. 5 for their locations). (A) Cross-stratified conglomerates lying on the basement substrate are erosionally truncated at their top by a highly irregular surface and overlain by very coarse-grained pebbly and shelly sandstones of Facies *A3*. The basement is not exposed here but is intuitively located less than few metres into the subsurface (car as scale is *ca* 2.5 m long). (B) Detail from the previous photograph showing poorly-sorted and well-rounded polymictic elements (hammer is 35 cm long). (C) Facies *A1*a showing cross-stratifications and being truncated by an irregular erosional surface (person as scale is 1.6 m tall). (D) Set of stratification planes locally dipping palaeo-landward.

sand–mud packages in mud-rich tidal systems (e.g. Visser, 1980). Tidal reversals in the strait in fact generate periodic changes in flow capacity, segregating grain populations by density/weight (i.e. siliciclastic/carbonate) within foresets during the stronger and weaker currents every six hours per day (e.g. Chiarella & Longhitano, 2012). Bundles of coarsening to fining-upward inclined lamina intervals also preserved within foresets (Fig. 16C) may reflect longer tidal periodicities of neap–spring tidal cycles, whereas reactivation surfaces interrupting regular foreset sequences would record slack-water stages separating two successive flood–ebb tidal phases (Longhitano & Nemec, 2005).

The dominance of trough cross-strata records the accretion of large, sinuous-crested, subaqueous three-dimensional dunes migrating under dominantly unidirectional tidal currents. The subordinate tidal phase may have been too weak to produce sand transport and bedform accretion in an opposite direction. Therefore, slack-water tidal stages may be recorded only by reactivation surfaces, with the overlying conformable foresets representing current reprises (Longhitano & Chiarella, 2020). Compound dune architectures (Fig. 16A) are well-known to be the expression of long-term variations in the competence of tidal currents, triggering the accretion of secondary bedforms onto larger dunes (e.g. Anastas *et al.,* 1997; Olariu *et al.,* 2012). The highly bioturbated deposits recorded as finer intercalations within the cross-strata may represent 'toesets' or lateral fringes of the subaqueous dune fields, which are usually areas of lower bed-shear stress and sediment accumulation rate, more prone to be colonized by infaunal organisms. The deep erosional surfaces interrupting the monotonous repetition of cross-strata are attributed to local scouring, probably related to erosion exerted by episodic sediment bypass originated by river-derived gravity-driven currents flowing at high angle to the direction of dune migration (see Fig. 6 for palaeocurrent data). These erosional–depositional units within tidal cross-sets are designated as a diagnostic element in strait-fill successions

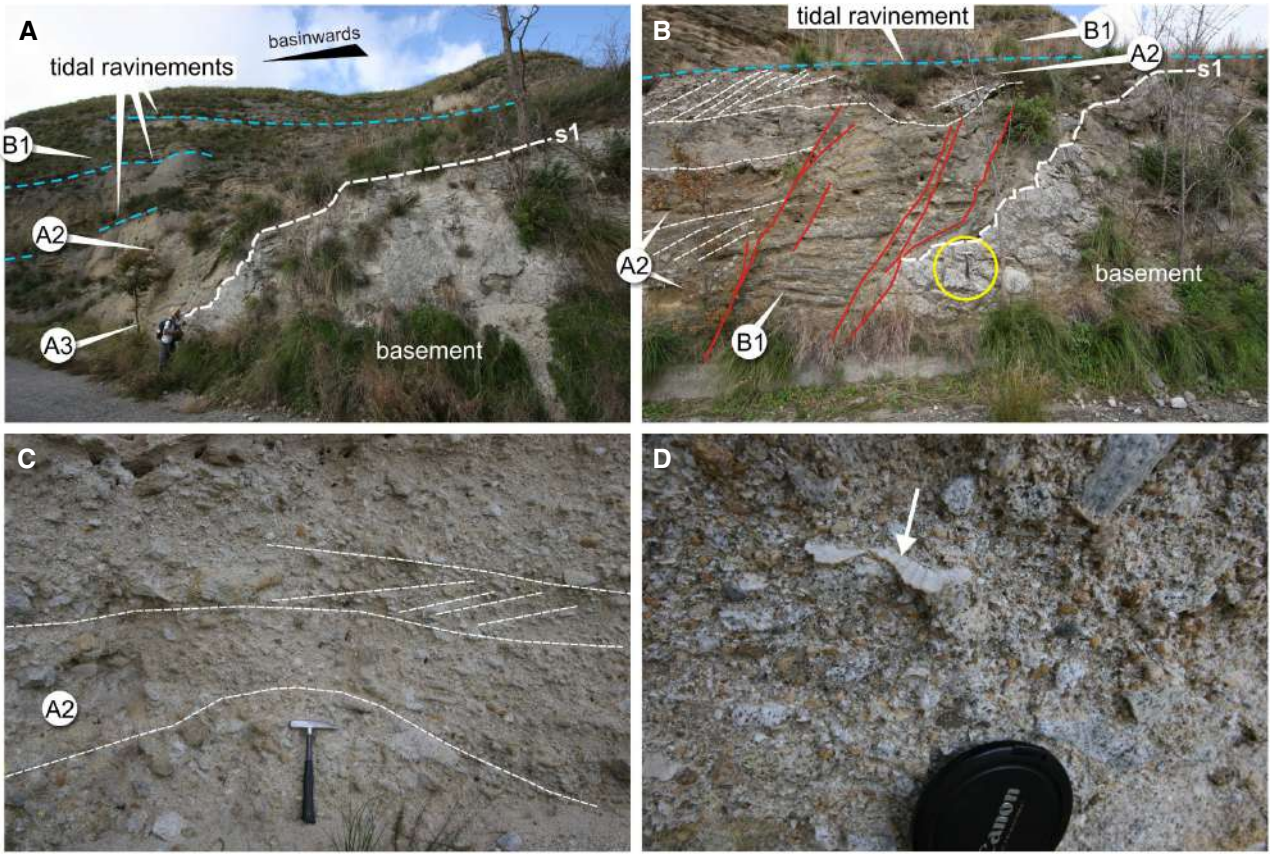

Fig. 8. Outcrop photographs of Facies *A2*. (A) Basal/lateral contact between the igneous basement (right) of breccia (*A2*), and the overlying pebbly sandstones (*A3*) and mixed arenites (*B1*). These latter lie on a low relief surface interpreted as a tidal ravinement. Sediment palaeo-transport inferred from facies *A3* and *B1* indicate directions oriented perpendicular to the section, suggesting that this contact would represent a side of a channel/canyon incised into the basement (person as scale is 1.7 m tall). (B) Detail from the previous photograph. Breccia of Facies *A2* are interbedded with mixed arenitic strata of Facies *B1* (s1 = base of the succession; hammer in the yellow circle is 35 cm long). (C) Detail of Facies *A2*. Although the general appearance is structureless, a poorly-defined planar-stratification can be recognized. (D) Monomictic gravel clasts associated with a fragment of a pectinid (arrow; lens cap is 6 cm in diameter).

as a consequence of proximity to unstable margins promoting mass-wasting processes (Longhitano, 2013, 2018a,b) or incipient canyons.

Facies *B2* – Tidal-influenced, strait-marginal, planar cross-stratified mixed arenites

Description

Facies *B2* represents the uppermost interval of Unit *B* and consists of 20 to 100 cm thick planar cross-strata bounded by low relief discontinuities (Fig. 17A and B). Sediments are mixed bioclastic–siliciclastic arenites with composition similar to that of underlying Facies *B1*, but with a higher *b/s ratio* (0.7 to 7.0), and including sparse intercalations of matrix-supported conglomeratic lenses (Fig. 17B). Bioturbation is widespread (B.I. = 3 to 4) and many intervals are completely homogenized by intense burrowing. Planar cross-strata dominantly exhibit 'simple' geometries (*cf.* Allen, 1980), i.e. including individual foreset units (Fig. 17C), rather than multiple foresets, as observed in the underlying 'compound' cross-bed sets. Cross-strata thicknesses range from 2 to 3 m in the west/north-west sector to 0.4 m towards the east/south-east (Fig. 17D), inferred to represent the distal and proximal depositional sectors, respectively. However, localized 40 to 50 cm thick trough cross-strata occur (Fig. 17E). The proximal to distal thickening trend of cross-stratification is associated with an increase in the B.I., which attains highest values near marginal areas.

Upward, tabular cross-strata of Facies *B2* grade into a monotonous succession of thinner strata (0.4 m thick, on average) lapping and back-stepping ESE-wards onto the block-faulted basement margin (Fig. 17A). Palaeo-flow indicators acquired in the small tidal foresets show dominant trends to the west/north-west and north-west.

Interpretation

The vertical stacking from three-dimensional (Facies *B1*) to two-dimensional (Facies *B2*) tidal cross-stratification records a general decrease in bed-shear stress through time (e.g. Southard, 1991; Longhitano *et al.,* 2014). Lenticular conglomeratic intercalations and small channel fills (Figs 15A and 17B) indicate occasional fluvial discharge, scouring local gullies into the top of the tidal bedforms and descending downslope for short distances. The recurrent 'simple' architecture of the tidal foresets (Fig. 17C and D) suggests more stable current patterns, whereas the overall decrease in set thickness towards the margin reflects a cross-sectional energetic trend typical of straits. In the absence of relevant coastal indentations, tidal currents are indeed faster along the strait axis, whereas they tend to decelerate towards the margins, due to the frictional effect of the shallower bottom on the tidal waves (Longhitano, 2018b; Longhitano & Chiarella, 2020).

Planar cross-strata of Facies *B2* record aggradation during the superimposition of straight-crested, subaqueous, two-dimensional dunes migrating under prevalently unidirectional currents, which were less energetic compared with those responsible for underlying three-dimensional dunes (Facies *B1*). This process-regime change is associated with the decrease in siliciclastic fraction in the mixed deposits of Facies *B2*, and to their back-stepping architecture onto the faulted margin. Due to their position in the stratigraphic succession, the tidal dune-bedded interval (Unit *B*) represents the distal frontal environment of the delta system, laterally adjacent to its proximal sectors represented by the deposits preserved in Unit *A*. Facies *B2* records a late transgressive stage, characterized by weaker tidal circulation related to an enlargement in the cross-sectional area of the strait (e.g. Chiarella *et al.*, 2012; Longhitano *et al.,* 2014, 2021; Longhitano, 2018b). The presence of shallow channels filled by coarse-grained material supports the interpretation of a subaqueous area connected to delta distributaries. Dunes of Facies *B2* are even richer in bioclasts, indicating that tidal currents favoured colonization of the soft bottom by organisms adapted to energetic conditions, or that tidal currents were sweeping adjacent areas (i.e. *near situ*) of high carbonate production. This type of setting seems to be a prerequisite for the development of carbonate factories in modern and ancient bedform fields subjected to current winnowing (e.g. James *et al.*, 2014). The net direction of tidal transport, suggested by the dominant west/north-west-oriented dip of tidal-bedform foresets, is parallel to the orientation of the western palaeo-margin of the ancient Messina Strait, which roughly corresponds with the master fault bounding this part of the basin.

DISCUSSION

Deltaic versus tidal process interplay at the head of a subaqueous strait canyon

The observed facies associations indicate that river outflow mixed with tidal currents, representing a persistent background process along the marginal area of the ancient Messina Strait. Interactions between hyperpycnal flows and tidal currents have been observed offshore modern tide-influenced and tide-dominated deltas (e.g. Wang *et al.,* 2010; Ayranci *et al.,* 2012). However, in this type of setting flood and ebb tides approach the shoreline perpendicularly; by contrast, in marine straits undergoing tidal amplification, tidal currents act as a contour flow moving parallel to the strait margins and influencing sublittoral sediment distribution (Longhitano & Chiarella, 2020). Examples of interplay between deltas impinging tidal straits and tidal currents have been documented recently from ancient strait-fill successions (e.g. Longhitano & Steel, 2016; Rossi *et al.,* 2017; Telesca *et al.,* 2020). The subaqueous delta-front deposits are reworked into tidal dune fields that migrate at high angle with respect to the direction of delta progradation. In addition, the progressive deflection of the delta lobe in the direction of the dominant tidal phase is another distinctive effect, eventually causing the possible detachment of sedimentary bodies from the main deltaic deposits (Keller & Richards, 1967; Galloway, 2002). During periods of low river discharge, fluvial deposits accumulated in the shallow-marine realm are thus subject to reworking by tidal circulation.

Palaeocurrent directions measured in the cross-stratified deposits of Unit *B* have a

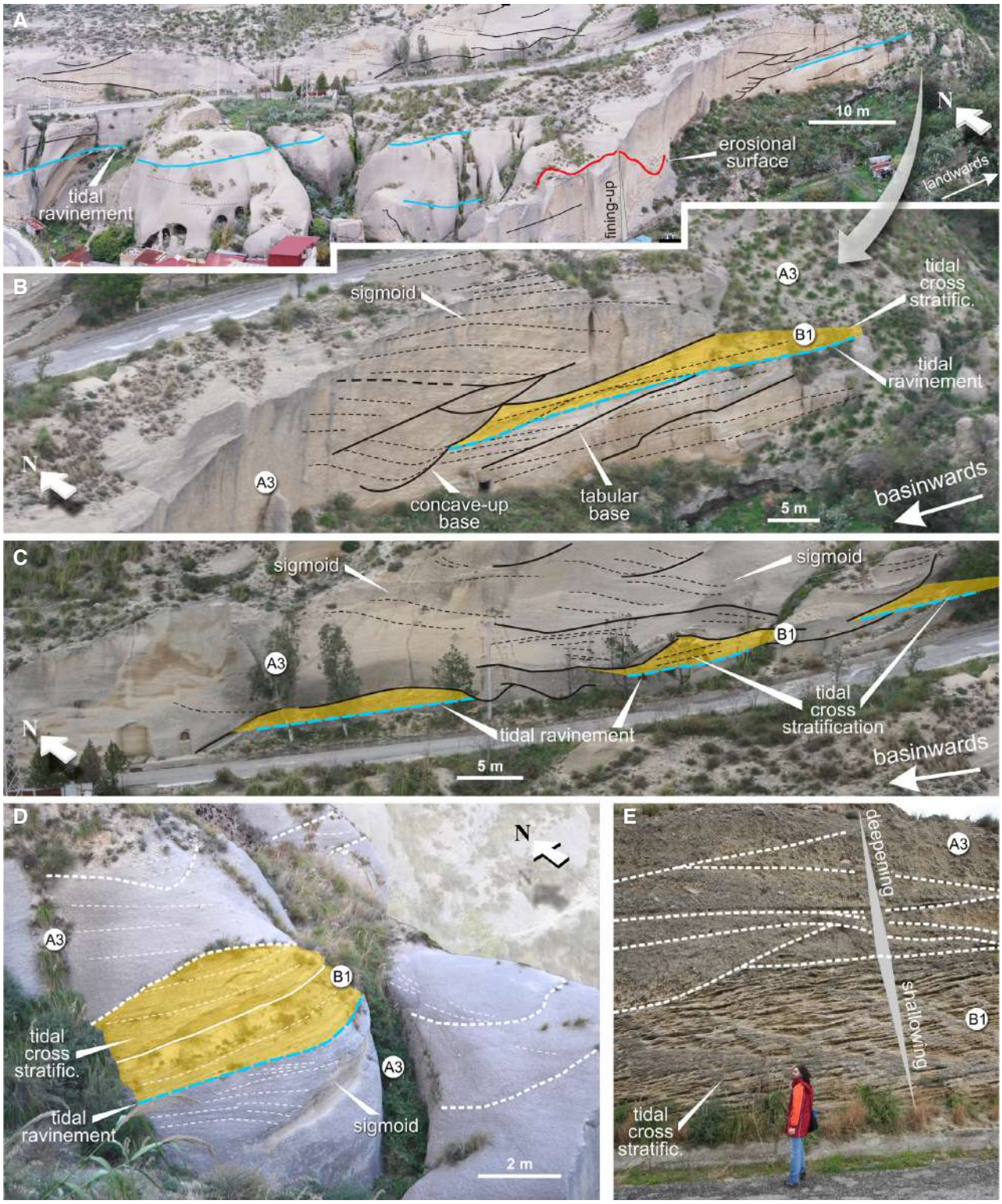

Fig. 9. (A) Deposits of Facies *A3* at the base of the dip-parallel cliff of the Calanna section (see location of the photographs in Fig. 5B). (B) Complex cross-cutting foreset units aggrading and back-stepping up-slope, comprising remnants of tidal biocalcarenites of Facies *B1* overlying a low relief ravinement. (C) Detail of internal foresets, which indicates downslope and upslope sand-body migration. (D) Detail showing the intercalation of tidal cross-stratified biocalcarenites of Facies *B1* intercalated within pebbly sandstones of Facies *A3*. (E) Close-up view of one of the observed contacts between Facies *A3* and the underlying Facies *B1* (person as scale is 1.8 m tall).

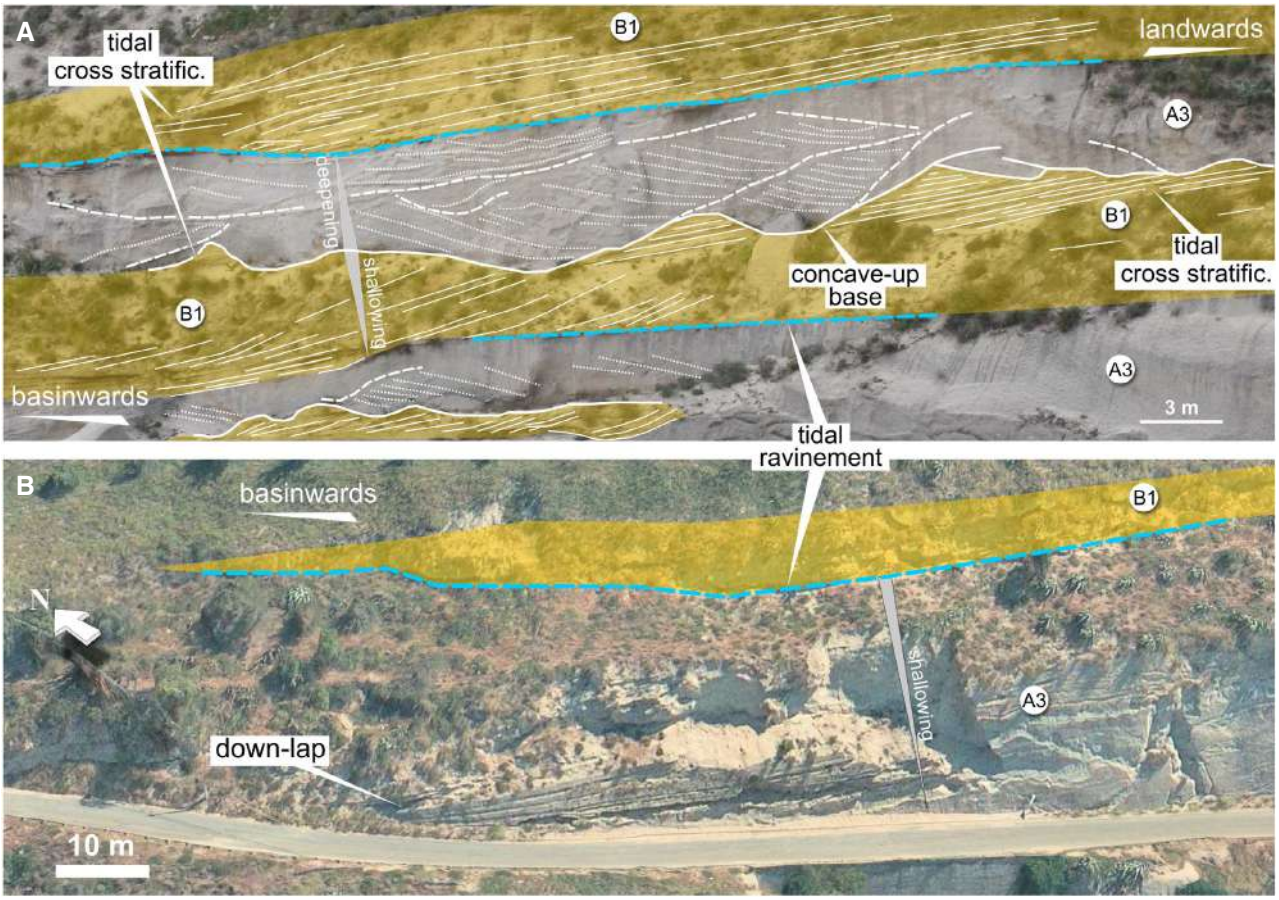

Fig. 10. (A) Multiple scour-and-fill structures in pebbly sandstones and conglomerates of Facies *A3* interpreted as cyclic steps and intercalated with cross-stratified tidal mixed bioclastic–siliciclastic arenites of Facies *B1*. Note second-order erosional surfaces displaying channel-shaped, concave-up geometry, with symmetry axis skewed upslope and cross-cutting relationships. Internal backset units, when fully preserved, show dominantly landward-prograding, subordinately aggrading, sigmoidal geometry. Where unaffected by internal, lower-rank (third-order) discontinuities, individual sigmoidal packages grade upwards into concave-up stratification. (B) Panoramic view of a section located *ca* 200 m basinward with respect to the insert 'A' and showing strata converging and indicating down-lap termination (see location of the photographs in Fig. 5B).

dominant unidirectional (north/north-west-directed) orientation because that area likely occupied the marginal segment of one of the two depositional zones of the strait (i.e. the strait-bedded zones, *cf*. Longhitano, 2013, 2018b). In modern tidal straits, this zone lies down-current of the strait centre. After the flow accelerates through the narrowest or shallowest strait cross-section, it expands and decelerates with a flood or ebb component that is always stronger than the opposite one. These current velocity variations generate a marked tidal asymmetry, a rapid decline in flow transport capacity, and the accumulation of sandy bedform fields reflecting the locally dominant tidal phase (Longhitano & Chiarella, 2020).

Reconstruction of the canyon-head system

The depositional scenario reconstructed for the studied sections can be referred to a proximal deltaic setting or a 'base of scarp' environment (e.g. Chiarella *et al.,* 2020) located at the entrance of a subaqueous canyon system. The first hypothesis is based on the observation of mouth-bar conglomerates (Facies *A1*) that, although with immature textural features, exhibit cross-stratification typical of proximal delta front, where also coarse-grained deposits are shaped into bars, because of the effect of fluvial inertial transport (Postma, 1984; Kazanci & Varol, 1990; Orton & Reading, 1993; Van Yperen *et al.,* 2020). The second hypothesis is indicated

Fig. 11. Outcrop photographs of Facies *A3*. (A) Crude inclined stratification in pebbly sandstones (person as scale is 1.6 m tall). (B) Detail of the pebbly sandstones, including gravels up to 4 cm in diameter. (C) Aligned, platy shell fragments indicating faint low-angle lamination (coin is 2.5 cm in diameter). (D) Detail of distally (west/north-west)-located, coarse-medium sandstones of Facies *A3* including large blocks derived from Facies *A1* and *B1*. (E) Undulate, cross-stratified sandstones and conglomerates, interpreted as swales and antidunes [person as scale is 1.7 m tall; see Fig. 5B for the location of panels (D) and (E)].

by the absence of wave-related sedimentary structures at the top of the channelized deposits, replaced by facies clearly indicative of unidirectional tidal reworking (Chiarella *et al.,* 2020). The preservation of tidal deposits points to a relatively deep (i.e. below wave base) setting dominated by tidal currents during prolonged intervals of minimal or no river outflows and may indicate an accumulation area detached from delta-plain deposits, which in fact have not been identified in the studied outcrops.

Common to both the proposed reconstructions of proximal subaqueous deltaic versus base of scarp setting is the presence of a canyon-head system,

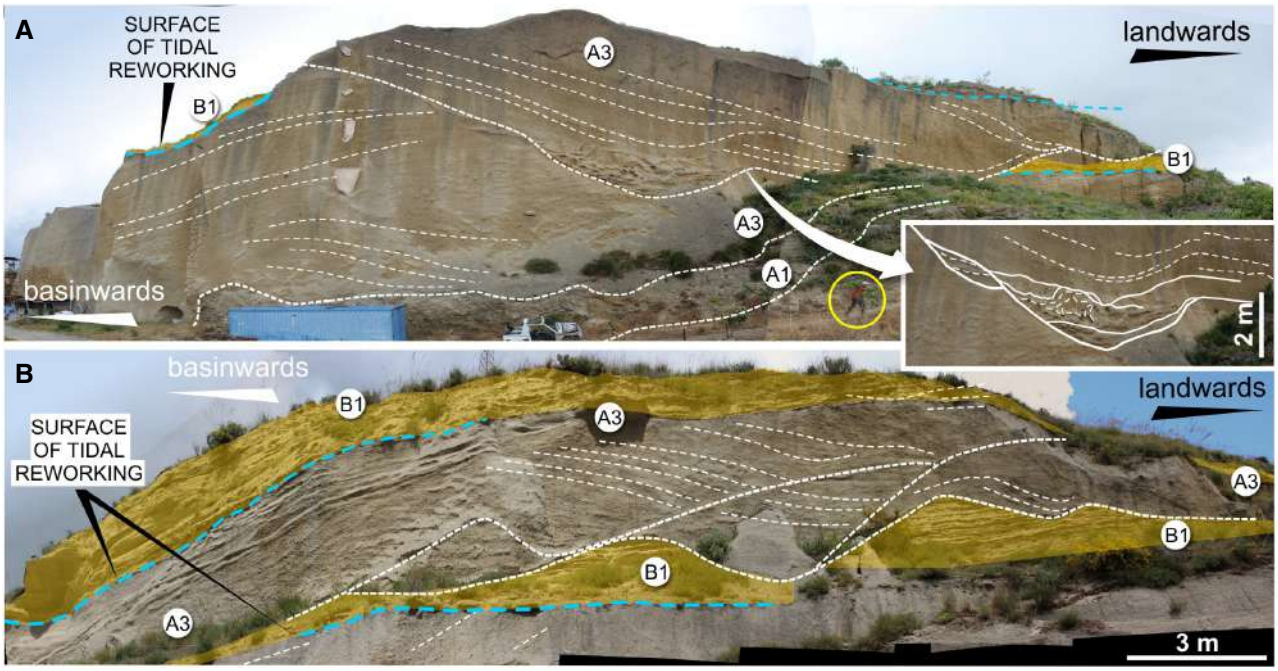

Fig. 12. Motifs of cross-stratification observed within two intervals of Unit *A* (see Fig. 5B for location). (A) A few metres above the basal contact over Facies *A1*, pebbly sandstones of Facies A3 exhibit cross-cutting discontinuities comprising backsets dipping up-slope. Soft-sediment deformation structures are also present (inset), possibly reflecting local collapses due to the steepness of the scour margins (person in the circle is 1.90 m tall). (B) Backsets of Facies *A3* show regular and repetitive scour geometries, and scoop into the underlying deposits of the same facies or cross-bedded mixed arenites of Facies *B1*, defining asymmetrical scours with profile steeper downslope but migrating up-slope. In both examples, channel tops are bounded by a reworking surface representing a tidal ravinement.

composed of minor subaqueous channel indentations close to the shoreline, and initially incised onto the basement. In this study, canyon heads were reconstructed by mapping the deposits of Unit *A* (see Fig. 4A), whose lateral distribution indicates several entry points to the system for sediment, likely forced by some degree of lateral confinement (Fig. 18A). These substrate incisions formed the proximal portions of a more extensive subaqueous sediment-transfer system into the basin, as recognized in modern base of slope settings (e.g. Galloway, 1998; Fig. 18B). The occurrence of canyons directly connected to the shoreline suggests that the sublittoral zone of this segment of the northeastern margin of the ancient Messina Strait was likely characterized by a very narrow or nearly absent shelf, as observed along those parts of the modern strait where tectonics has been active until recent times (see Fig. 2A to D).

The steep bathymetric gradient was related to the morpho-tectonic setting of this fault-controlled margin and formed an important prerequisite to favour supercritical conditions for river-fed hyperpycnal flows, generating repeated processes of scour and fill in which aggradation was, at least at times, controlled by fields of large, up-dip migrating bedforms, identified here as cyclic steps.

In Fig. 18B, the reconstructed palaeo-environmental setting suggests the presence of at least four canyon branches or indentations, eroding and retreating towards the shoreline. These correspond roughly with the branching pattern of the large-scale scour-fills observed in the Calanna succession. The exposed strata, which are today comprised between a series of hills separated by subaerial incisions, thus represents a case of 'inverted topography', i.e. deposits originally occupying the topographic lows today form a positive relief or hillcrests.

For each of the subaqueous canyons, the existence of a river mouth is supposed to have been the main source of sediment discharge into the canyons. However, erosional canyon heads with no rivers at their subaerial end are observed today in many parts of the modern Messina Strait

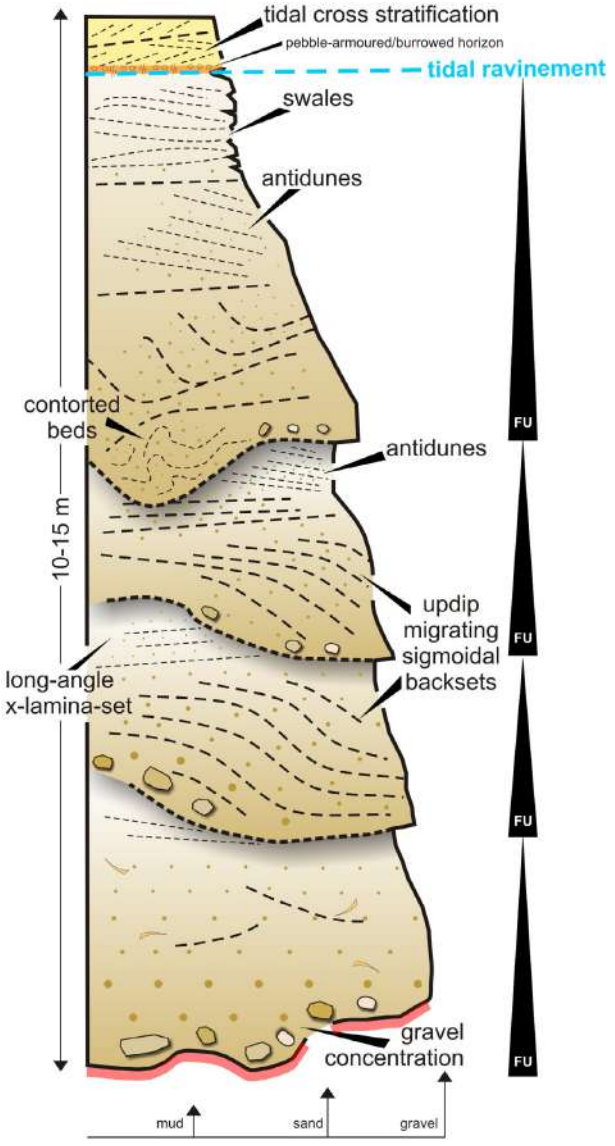

Fig. 13. Reconstructed, vertically stacked sequence of sedimentary structures observed within individual gravelly sand bodies of Facies *A3*. The base (first-order discontinuity) is erosional and associated with sparse pebble and cobble clasts deriving from the substrate. Individual bodies comprise a variable number of fining-upward (FU, amalgamated) intervals, in turn bounded by second-order discontinuities. Internally, backsets have sigmoidal to angular geometry and migrate mostly upslope. The tops of these intervals comprise up-dip migrating strata and swales. The very top of the sand body is marked by a ravinement surface and is overlain by tidal cross-bedded facies.

(Fig. 2B to D). Although these features have no direct sediment supply, it is interesting to note how they also contain supercritical bedforms migrating upstream with dynamics extremely similar to those of river-fed canyon heads (Casalbore *et al.,* 2014, 2019). Arguably, deposits within these canyons may derive from longshore-transported sediments (Fig. 18B) that, once captured within the canyon, are subsequently involved in mass-wasting instability and occasional generation of high-energy turbidity currents (Green *et al.,* 2007; Di Celma *et al.,* 2010).

Supercritical-flow processes within shallow-marine canyons

The hypothesis that delta lobes entered canyon heads in the strait-margin nearshore zone is suggested by the contiguity of the coarse-grained facies of Unit *A* to the basement margin, the abrupt lateral (along-strike) pinching out of the succession, and the presence of basal mouth-bar conglomerates (Facies *A1*) and marginal breccias (Facies *A2*).

During the first phase of canyon infilling, sediment accumulation may have occurred through stages of erosion/deposition, recording the progressive depletion of the current energy after every episode of river discharge. This interpretation is based on the observation of recurrent depositional architectures, commonly documented in the various bed-sets composing Unit *A* (Fig. 19), including the different hierarchical orders of erosional discontinuities.

Episodic, high-energy flash-floods caused by heavy rainfall events and interrupting relatively protracted periods of minimal discharge are common to present-day fluvial environments of the region (e.g. Sorriso-Valvo & Terranova, 2006; Sorriso-Valvo, 2008; Lo Iacono *et al.,* 2017), reflecting the recent and modern climate background of southern Italy and of the southern Mediterranean, more in general. The combination of high-relief and limited area of local catchments, are additional elements for generating quick and amplified hydrograph responses to precipitation events (Patton, 1988; Ventra & Clarke, 2018). Rates of subaerial erosion are high in these dryland coasts, and sediment yields are known to be amongst the highest globally, particularly in Mediterranean regions (Hooke, 2019). Along the coasts of the Messina Strait, river valleys are often in direct hydraulic continuity with subaqueous canyons, whose heads are located less than 50 m away from the modern shoreline, and rapidly retreating (Casalbore *et al.,* 2014, 2017; Gamberi *et al.,* 2017). On the occasion of heavy and localized rainfall concentrated onto small catchment sectors of the coast,

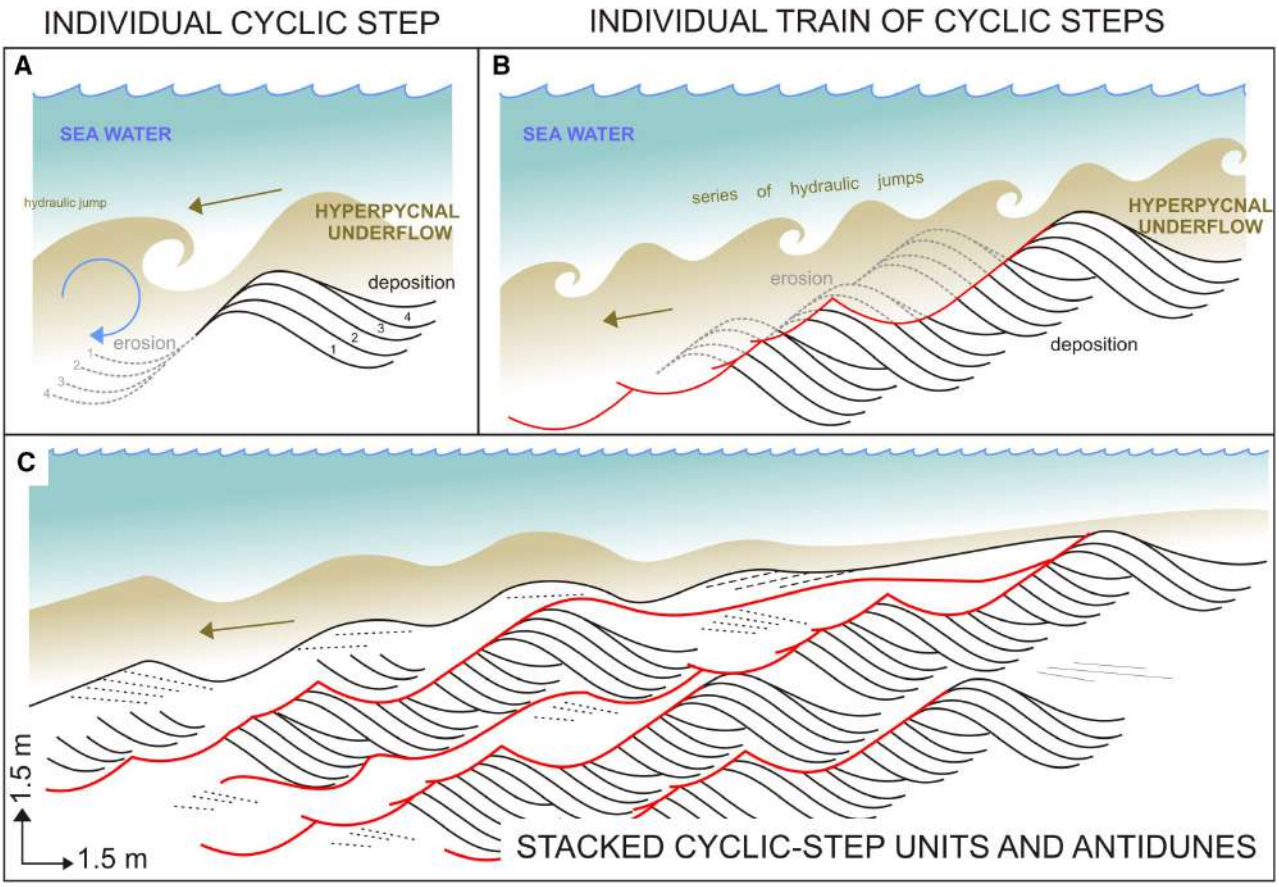

Fig. 14. Genetic processes inferred for the origin of the large-scale cyclic steps observed within the deposits of Facies *A3*. (A) Individual backset units represent a single hydraulic jump occurring at the interface above a hyperpycnal flow propagating downslope. This process causes erosion of previously deposited strata and contemporaneous accretion of upslope migrating backsets (numbers indicate the sequence of bed erosion/deposition). (B) Trains of hydraulic jumps cause repeated sequences of cyclic steps and the formation of an erosional contact deriving from the amalgamation of erosional surfaces scoured by migrating hydraulic jumps. (C) Stacked units comprising subsequent generations of cyclic steps resembling the architectures observed in outcrop. In this last sketch, the hyperpycnal current flows with weaker energy, generating antidunes over underlying cyclic steps (inspired after Cartigny *et al.,* 2011, 2014).

the unstable margins of steep subaerial canyons may rapidly collapse, generating high rates of sediment discharge, transferring thousands of cubic metres of bedload towards the shoreline (Langbein & Schumm, 1958; Dedkov & Mozzherin, 1992). Hence, in such high-relief flash-flood-prone settings, sediment-laden discharge events are prone to generate density currents that transfer significant volumes of debris rapidly from the subaerial to the subaqueous portion of the system (e.g. Warrick & Milliman, 2003; Warrick *et al.,* 2008; Katz *et al.,* 2015).

The effect of river floods onto the most proximal subaqueous zone of the coast is concomitantly erosional and depositional (Fig. 19). Scouring of chutes within the canyon is associated with canyon-head receding, whereas episodic accretion of trains of large supercritical-flow bedforms migrating upstream (e.g. Casalbore *et al.,* 2011, 2019; Tubau *et al.,* 2015) is facilitated by the tendency of density currents to rapidly attain high densimetric Froude numbers along steep bathymetric gradients (Komar, 1971; Sequeiros, 2012). These processes are common in deep-water slope and channel/canyon settings, and are particularly known for channel–lobe transitions at the base of continental slopes (e.g. Wynn *et al.,* 2002; Postma *et al.,* 2016, 2021; Covault *et al.,* 2017; Ono & Plink-björklund, 2018; West *et al.,* 2019). Fields of supercritical-flow

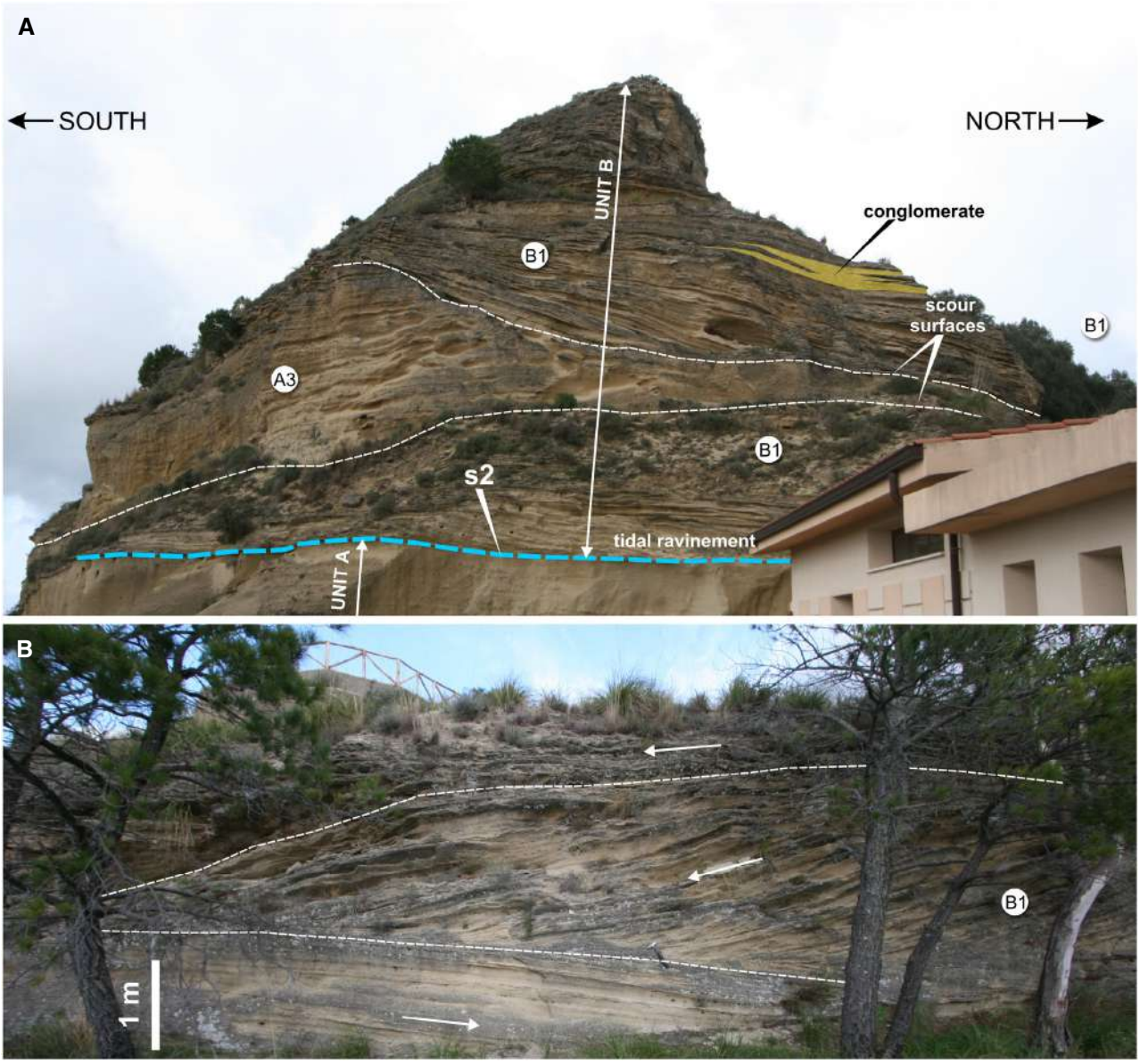

Fig. 15. (A) Contact separating the top of Unit *A* and the base of Unit *B* (see Fig. 5B for location). Here, erosional discontinuities have cross-cutting relationships, whereas cross-stratified mixed arenites of Facies *B1* include local conglomeratic lenticular intercalations (s2 = Unit *A*/Unit *B* boundary). (B) Outcrop of Facies *B1* oriented perpendicular with respect to the basinward direction and showing tidal foresets with apparent opposite direction of migration (arrows) but reflecting a net direction of sediment transport perpendicular to the road cut, as typical for three-dimensional dunes

bedforms fed by flood-prone river outflows have been documented along subaqueous portions of modern deltas in other areas of the Mediterranean (e.g. Urgeles *et al.,* 2011; Lobo *et al.,* 2015; Casalbore *et al.,* 2017; Kostic *et al.,* 2019). Outcrop examples have been recently reported from an ancient channel–lobe transition zone of a deep-water delta, from Eocene continental-slope successions of southern California (Ono & Plink-björklund, 2018), in the Eocene of north-eastern Spain (Postma *et al.,* 2021), and in Plio-Pleistocene base of scarp deposits exposed in a southern sector of the western margin of the Messina Strait (Longhitano, 2016; Chiarella *et al.,* 2020). In particular, Postma *et al.* (2021) observe a composite, undulate basal discontinuity filled by

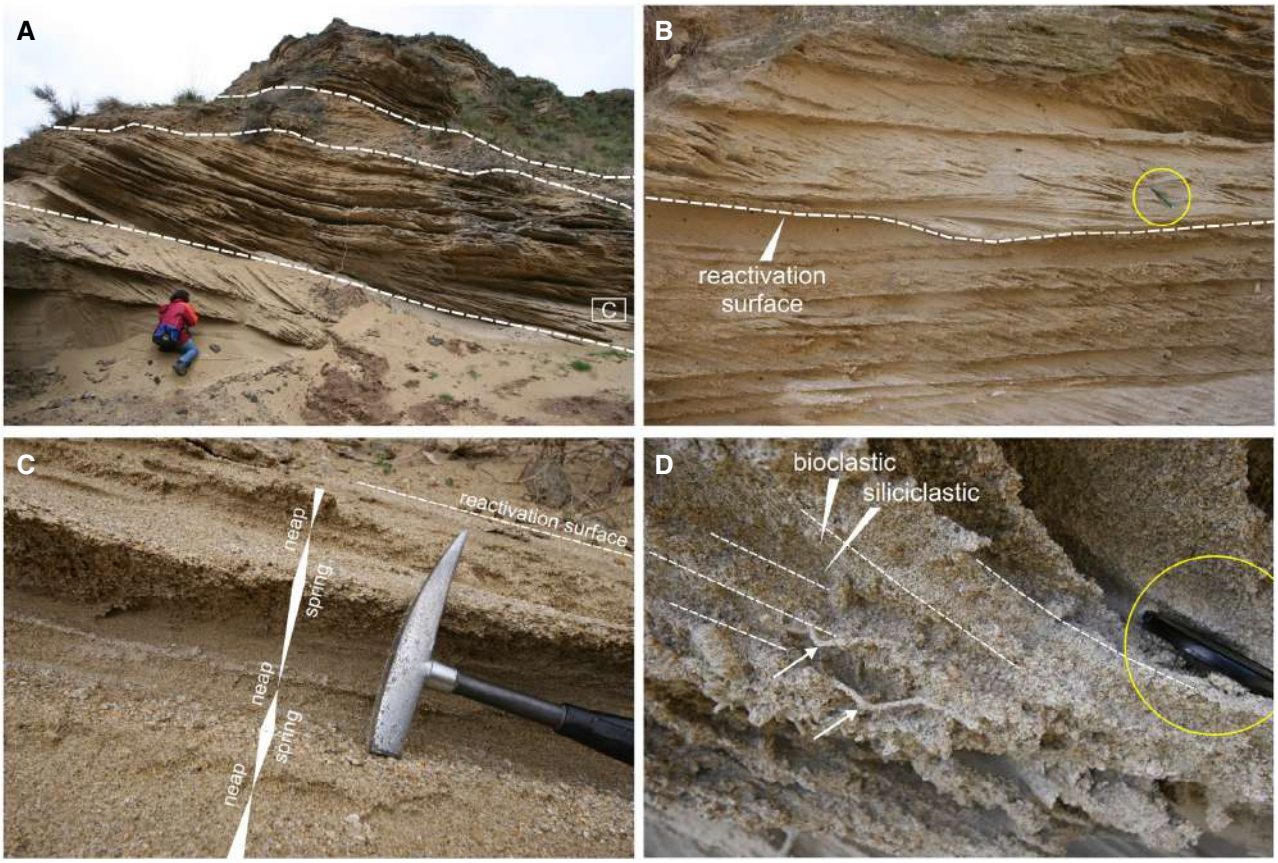

Fig. 16. Outcrop photographs of Facies *B1* showing internal details of cross-strata. (A) 'Compound' cross-strata, consisting of several horizons of superimposed bedforms migrating over the frontal (lee) side (surface inclined to the right) of an underlying larger dune (migration direction to the right; person as scale is 1.8 m tall). (B) Internal reactivation (scoured) surface, separating superimposed foresets (pencil for scale in the circle is *ca* 14 cm long). (C) Detail from the previous photograph showing neap–spring tidal bundles, consisting of repeated coarsening to fining-upward pair of laminae. (D) Lamina-scale siliciclastic/bioclastic rhythms are often amalgamated by burrowing (arrows), here attributed to *Thalassinoides* (lens cap for scale is *ca* 6 cm long).

repeated internal channel deposits, scouring the adjacent channels and migrating upslope, suggesting a process of retrogressive erosion (see Fig. 14). This process was likely responsible also for deposition of Facies *A3*, through a continuous reshaping of upslope-migrating backset beds and contemporaneous truncation of underlying deposits, until a definitive transition to subcritical conditions at flow waning stages. The topmost depositional record of density-current events was successively reworked by tidal currents (Fig. 13).

Sequence-stratigraphy of the transgressive delta–canyon complex

The studied succession shows a stratigraphic assemblage indicative of subaqueous deltaic deposits accumulated during an overall rise of the relative sea-level, with periods of minor falls and stillstand (e.g. Postma, 1995). A relative sea-level curve is reconstructed in Fig. 20 by considering the low relief master discontinuities observed in outcrop and assessed in the correlation panel (blue lines in Fig. 5B) as ravinement surfaces (Swift *et al.,* 1987). Flat stratigraphic discontinuities preserved in marginal-marine strata commonly refer to erosion by surface waves on narrow shelves, forming wave-cut platforms (e.g. Cattaneo & Steel, 2003). In the present case, the depth of the deposits inferred below base level and the occurrence of overlying tidal cross-strata of Facies Association B suggest that these surfaces are a type of tidal ravinement promoted by energetic tidal currents in a narrow marine strait setting (cf. Longhitano & Steel, 2016; Longhitano & Chiarella, 2020).

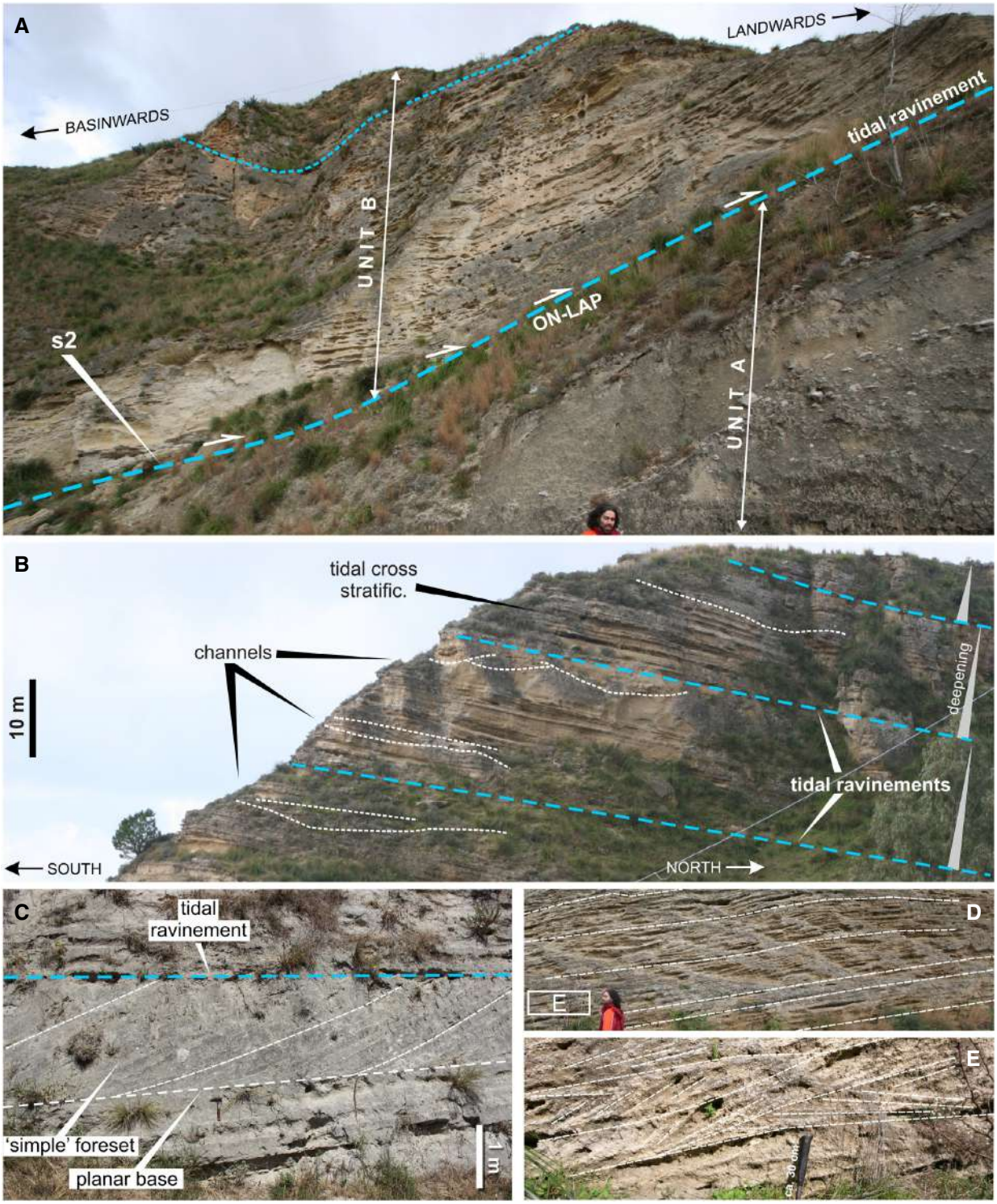

Fig. 17. (A) East/south-east uppermost termination of the WSW–ENE-oriented cliff of the Calanna Section, showing mixed arenitic strata of Facies *B2* (uppermost Unit *B*) erosionally overlying and back-stepping onto the top of the deposits of Unit *A* (s2 = Unit *A*/Unit *B* boundary; person as scale is 1.8 m tall). (B) Cross-strata geometries observed within Unit *B* are dominantly tabular and interbedded with 1 to 2 m thick channel deposits. (C) Planar-based, 'simple' foreset strata *ca* 1.2 m thick, grade up-dip into 0.2 to 0.4 m thick strata (D), reflecting a decrease in tidal-current competence from the strait axis to the strait margin (person as scale is 1.8 m tall). (E) Detail from the previous photograph, showing an example of trough cross-strata (Facies *B1*) whose palaeo-direction of migration is towards the cliff (see Fig. 5B for the location of the photographs).

The deltaic succession preserved at Calanna shows an initial progradational trend corresponding to Unit *A*, followed by a retrogradational stacking pattern represented by Unit *B*. In Unit *A*, the various wedges are comprised between master erosional discontinuities (f1 to f6, red lines in Fig. 20; see also Figs 7, 9 and 10), although remnants of original transgressive surfaces are still preserved, in places (see Fig. 9B and D as an example). These wedges can be regarded as simple sequences, based on the observation of their irregular/undulate erosional top indicating stages of minor sea-level fall without significant emergence. Strata packages composing Unit *B* are instead bounded by tidal ravinements or flooding surfaces (t7 to t11, blue lines in Fig. 20) showing a retrogradational trend. Unit *B* thus consists of back-stepping, stacked parasequences or 'amalgamated subtidal cycles' (*sensu* Goldhammer *et al.,* 1990). The progradational to retrogradational stacking pattern of units *A* and *B* records a phase of tectonically-induced transgression, and reflects a major change in the ratio between sediment supply and accommodation (*S* and *A* in Fig. 20, respectively). Internally to Unit *A*, each deltaic wedge represents transgressive–regressive (T–R) cycles, where the basal tidal-influenced deposits overlying the tidal ravinement are the transgressive counterpart, whereas the fluvial-influenced strata are the regressive one (see Fig. 9E, as an example). In places, especially where erosion exerted by fluvial outflows was strong enough to remove entirely the tidal transgressive interval, these cycles show only the regressive trends and are characterized by inclined strata downlapping onto the basal flooding surfaces or onto the top of the previous wedge (Fig. 10B). In the overlying Unit *B*, strata are organized into retrogradational parasequences, generally showing deepening-upward trends (see Fig. 17B, as an example). Unit *A* thus records the canyon infill

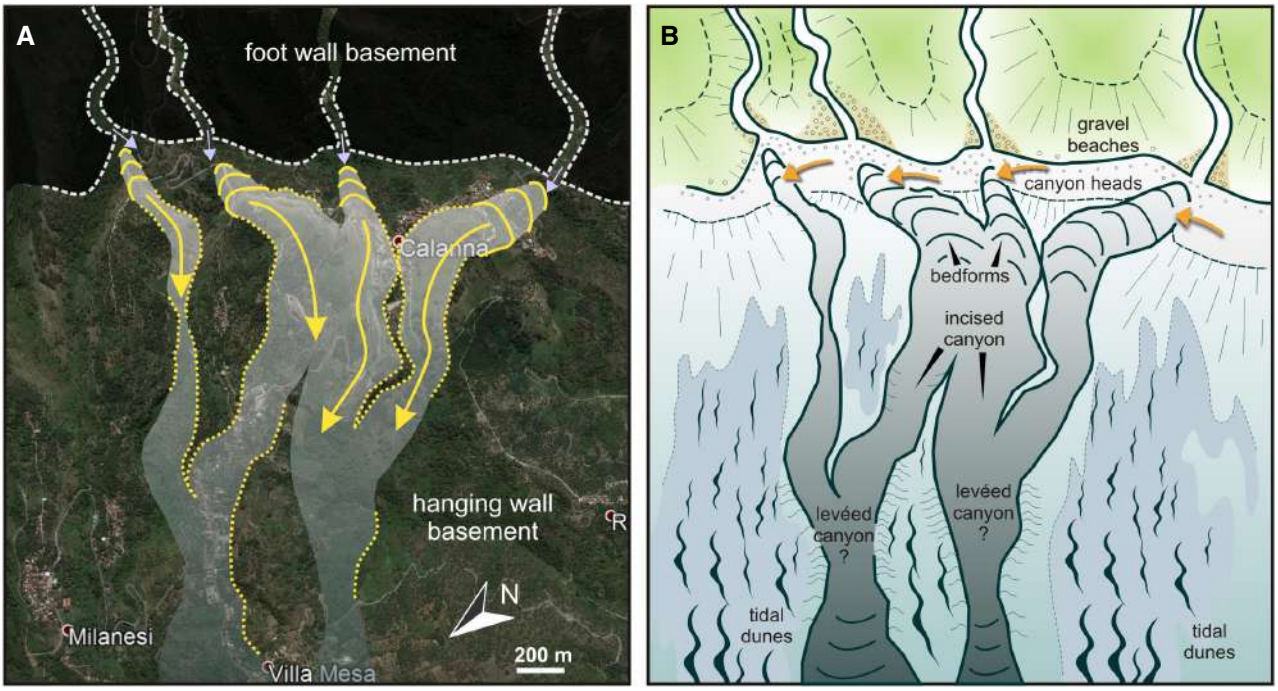

Fig. 18. (A) Aerial view of the modern relief of the studied sections. Yellow dashed lines indicate the lateral limits of the sandstones belonging to Unit *A*. These lines, traced based on the block-diagram presented in Fig. 4A, are inferred to correspond to the main boundaries of the canyons. Yellow arrows indicate direction of basinward sediment transport. The dashed grey line shows the inferred palaeo-shoreline and blue arrows indicate hypothetical small drainages supplying the canyons. (B) Reconstruction of the palaeo-setting based on the picture in (A). The multiple-branch canyon represents the subaqueous continuation of rivers and the proximal segment of a longer system of sediment transfer towards the deeper strait. Orange arrows indicate possible catchment of longshore drift sediment into the canyon heads. Tidal dunes reworked interfluves. Channel levées are supposed to converge basinward.

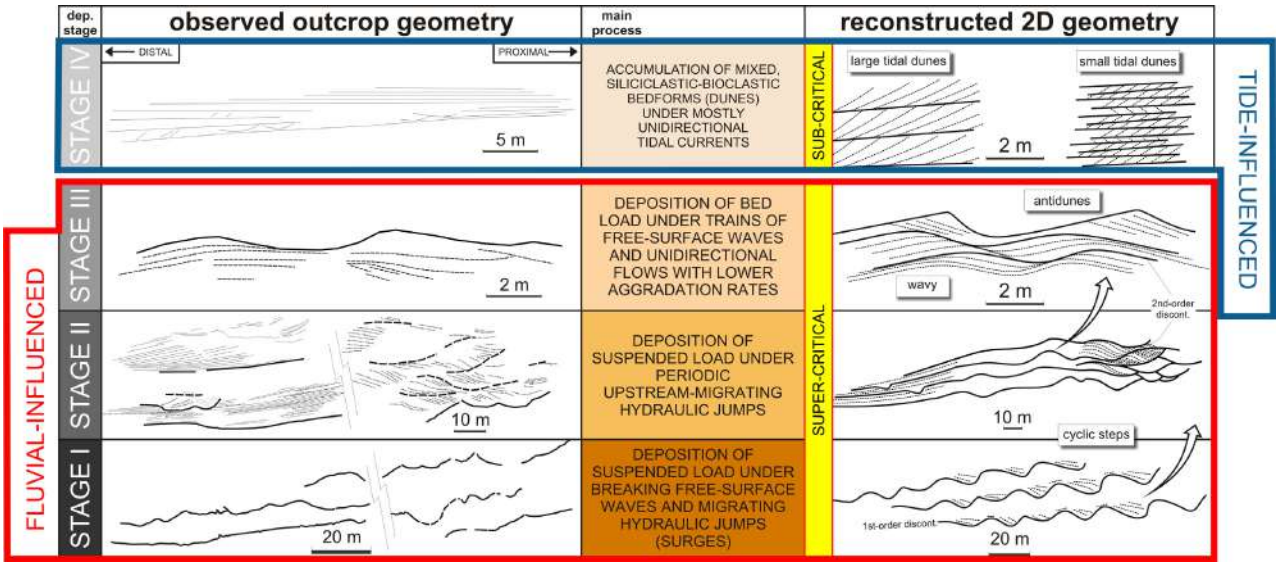

Fig. 19. Reconstructed depositional stages based on line-drawing of the architectural elements observed from outcrop. Stages I to IV record the evolution of each episode of river outflow entering the shallowly subaqueous coastal area, from a phase of very high energy and erosion, progressively towards phases of lower energy and deposition. Supercritical-flow conditions dominated during the first stages. Flows may have also evolved from Stage I to III, generating turbidity currents whose sedimentary record is presumably preserved more distally, in the basinal portion of the section.

during the early transgression, whereas Unit *B* represents the diffusion of strait-margin tidal dunes and a general delta-bottom flattening over the previous subaqueous incised topography during a late stage of transgression (Fig. 20). The general absence of wave-related sedimentary structures in the deposits of both Unit *A* and Unit *B* is indicative of deposition below the average fair-weather wave-base level, and of dominant tidal and gravity-flow processes which in time governed the formation of facies signatures. This interface in the Mediterranean is known to range nowadays between −15 m and −20 m of depth, based on modern measurements of the average wavelength in the area of the Messina Strait (Corsini *et al.,* 2003). No storm-wave traces have been recognized in the studied deposits. However, this does not exclude that strata of Unit *A* may have episodically been affected by energetic waves, but their sedimentary signature may have been reworked by tidal currents during pauses of fluvial-dominated activity.

Evolution of the Calanna canyon-head delta system

The analysis of the studied succession suggests a series of evolutionary stages for this segment of margin of the ancient Messina Strait. The coastal zone and related deltas may have lacked wide subaerial alluvial plains and well-defined distributary channels due to the high-relief setting, dominated by rocky coastal tracts, analogous to the modern-day physiography of the region. The sublittoral zone had high bathymetric gradients descending towards the deeper axial strait zone that connected the coast through a narrow shelfal belt composed of littoral drift sediments. Shallow canyon heads eroded into the basement, retreating towards the coastline and capturing sediment from longshore-drift systems at a short distance from the coast (Fig. 21A). Canyons probably originated from riverine incision related to a previous lowstand stage. Ephemeral rivers debouched episodically gravel-size deposits that were reworked locally into subaqueous mouth bars (Facies *A1*) by the combined action of waves and currents in the proximal sublittoral belt. More distally, tidal currents moulded fields of medium to small dunes (Facies *B1*; Fig. 21A).

Tectonic uplift increased the gradient enhancing canyon headward erosion (Fig. 21B), provoking localized collapses of basement portions (Facies *A2*) and favouring more efficient transport of gravel and sand by episodically river-triggered

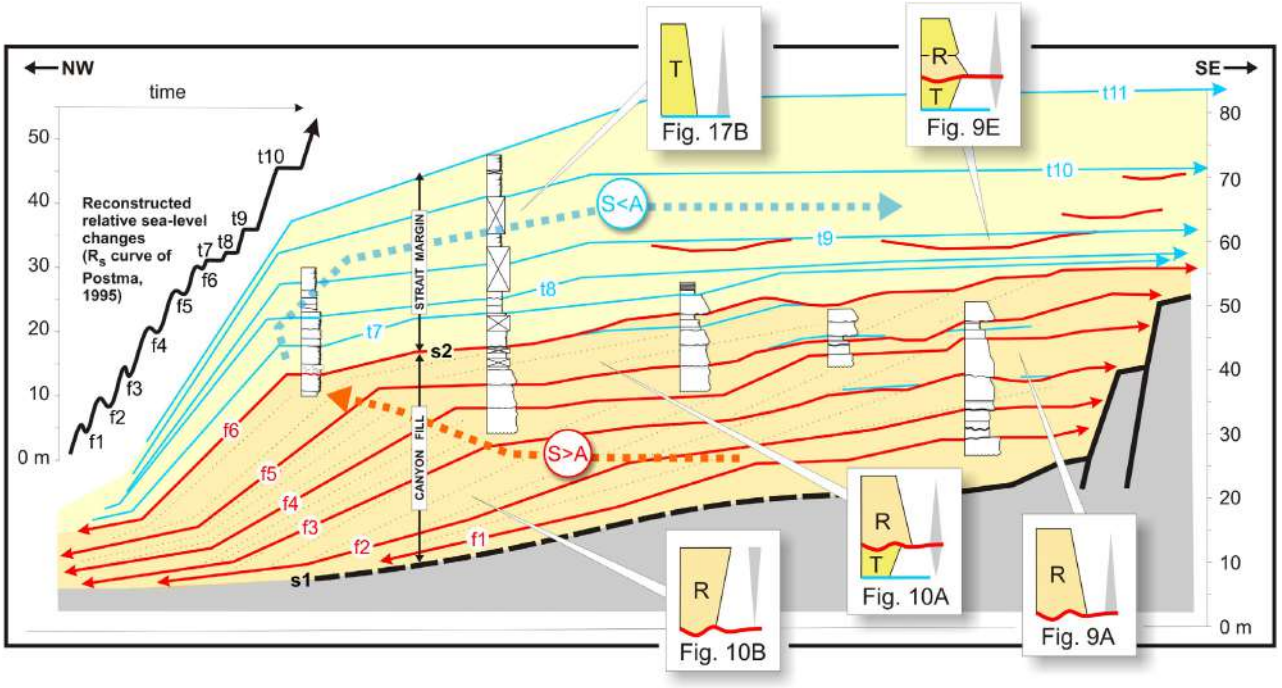

Fig. 20. Correlation panel reconstructed along the north-west/south-east oriented cliff of the Calanna section and showing the progradational trend of Unit *A* and the retrogradational trend of Unit *B* (dotted orange and blue arrows indicate delta clinoform trajectories), accumulated within the canyon-head system. The relative sea-level curve in the top-left corner shows a major rising trend punctuated by minor falls (f1 to f6) and stillstands (t7 to t11). The former have been inferred based on the depth of the erosional surfaces (in red), whereas the latter (in blue) are tidal ravinements and have been correlated to the height of their on-lap contacts (s1 = base of the succession; s2 = Unit *A*/Unit *B* boundary). Schematic logs indicate transgressive/regressive (T–R) cycles composing discrete parts of the succession (see the indicated figures for corresponding outcrop examples).

underflows (Facies *A3*). These latter supplied sediment during episodic flash-floods provoked by rainfall on steep mountainous local catchments (Fig. 21B). Jet-flows at the river mouth attained supercritical flow conditions along the proximal canyon tract and promoted the development and upstream migration of large crescentic bedforms (Fig. 21B). A final stage is inferred based on the predominance of tidal deposits forming the uppermost Unit *B* of the succession. The tectonically-induced subsidence of the hanging-wall margin induced a long-term transgressive trend with flooding of the previously incised river valleys (Fig. 21C). Consequently, the process of canyon-head retreat was possibly arrested, whereas tidal dunes (Facies *B2*) back-stepped into the block-faulted margin. However, river discharge never stopped entirely during transgression and the more proximal dune fields were occasionally excavated by riverine underflows and rapidly remoulded by tidal bedforms, represented by Facies *B2* (see Fig. 15A).

Implications for reconstructing deltas entering shallow-water canyons

The deltaic deposits documented in this study depart from standard facies and architectural models suggested for reconstructing ancient deltas from sedimentary successions (Fig. 22A). In spite of the continuity of exposure along the original depositional dip, there are no clearly recognizable large-scale clinoform architectures such as those typically produced by deltas entering tectonically controlled high-gradient settings (e.g. McPherson *et al.,* 1987; Nemec, 1990; Longhitano, 2008). This hampers the recognition of large-scale architectural subdivisions, such as topset, foreset and bottomset, and reduces the ability to identify genetically-related depositional sub-environments (e.g. Driscoll & Karner, 1999; Swenson *et al.,* 2005; Seybold *et al.,* 2007; Longhitano, 2008; Geleynse *et al.,* 2010, 2011). The over-thickening accumulation of strata during the transgressive stage contrasts with what

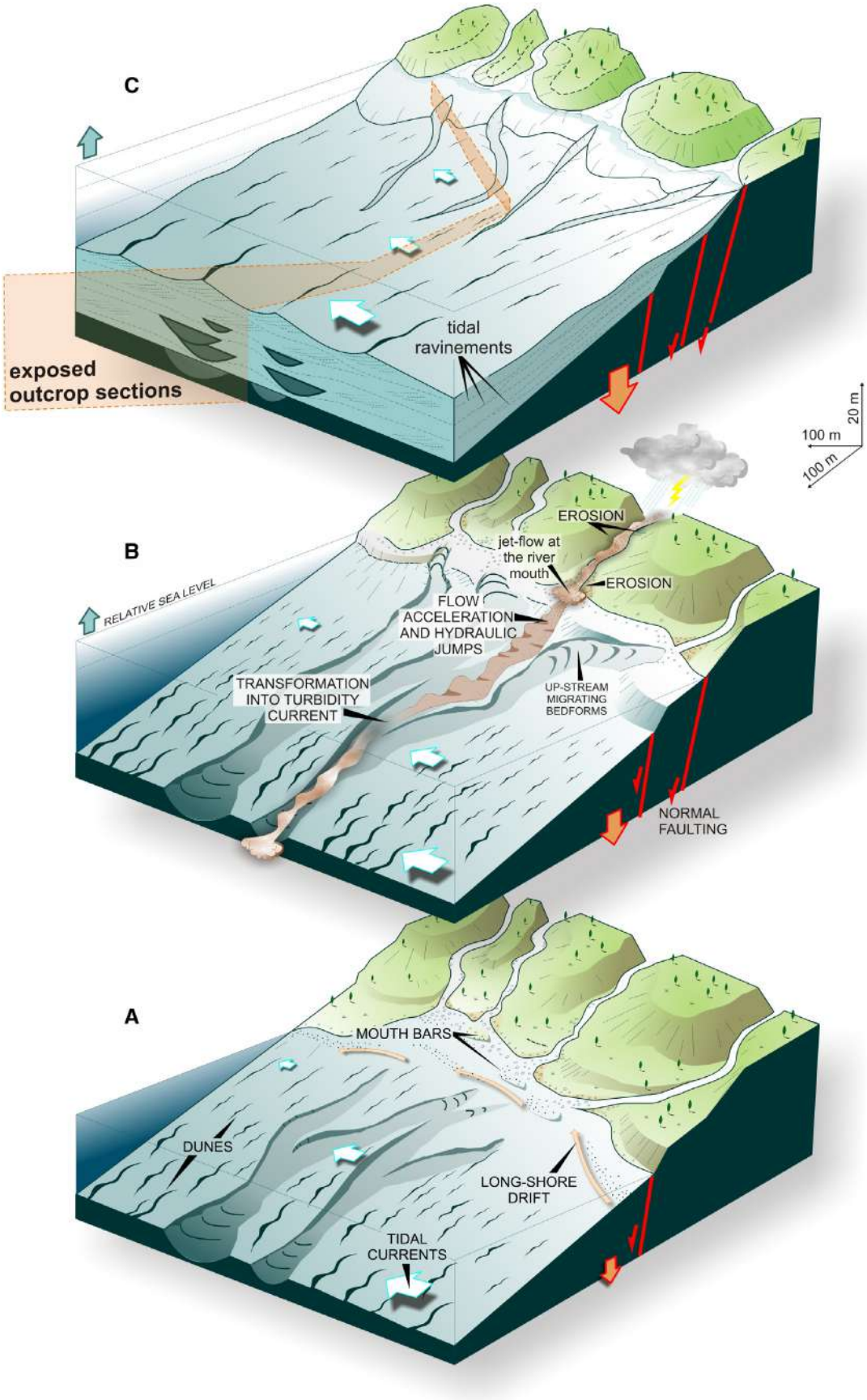

Fig. 21. Chronological sequence of the depositional scenario reconstructed for the studied area. (A) During the initial stage, riverine incision continued over the sublittoral slope into shallow canyons. Dunes occupy the inter-canyon zones. (B) As the faulting caused a stage of relative sea-level rise, the canyon recessed landward. Here, an episode of hyperpycnal flow is simulated with stages of current acceleration within the canyon entrance and resulting hydraulic jumps. Hypothetically, the same flow evolved into subcritical turbidity currents more distally. (C) Final stage of late transgression during which tidal dunes sealed the underlying canyon-fill sequences. Note ephemeral incisions excavated into the proximal dune field from occasional river activity during the latest stage of transgression.

was observed for Mediterranean Quaternary marginal-marine sequences, where the limited preservation of the transgressive intervals due to low rates of accommodation and reduced rates of sediment supply to the coast seem to have been recurrent factors (Lobo & Ridente, 2014; Ridente, 2016). In the present case study, over-thick transgressive strata are probably due to the combination of lateral confinement for the subaqueous portion of the deltas and to a lack of accommodation for delta plains, and represent another element that makes the application of standard deltaic facies and architectural models difficult to utilize in settings like the one described here.

New criteria for the characterization of deltaic successions entering a shallow-marine steep slope incised by canyon heads are provided here. The plan-view reconstruction of the distribution of fluvial-dominated facies (Unit *A*; Fig. 18A) points out that the delta initially split into multiple branches, represented by mouth bars or lobes, once entered into the sublittoral zone (Fig. 22B). This process prevented the attainment of the fan-shaped, radially axisymmetrical plan geometry characteristic of unconfined delta fronts due to the longshore redistribution of sediment exerted by waves and currents (Korus & Fielding, 2015; Fig. 22A). This major change in sediment distribution was mainly attributed to the capturing of sediment further into the basin by the nearest canyon-heads, and may thus justify the sinuous aspect

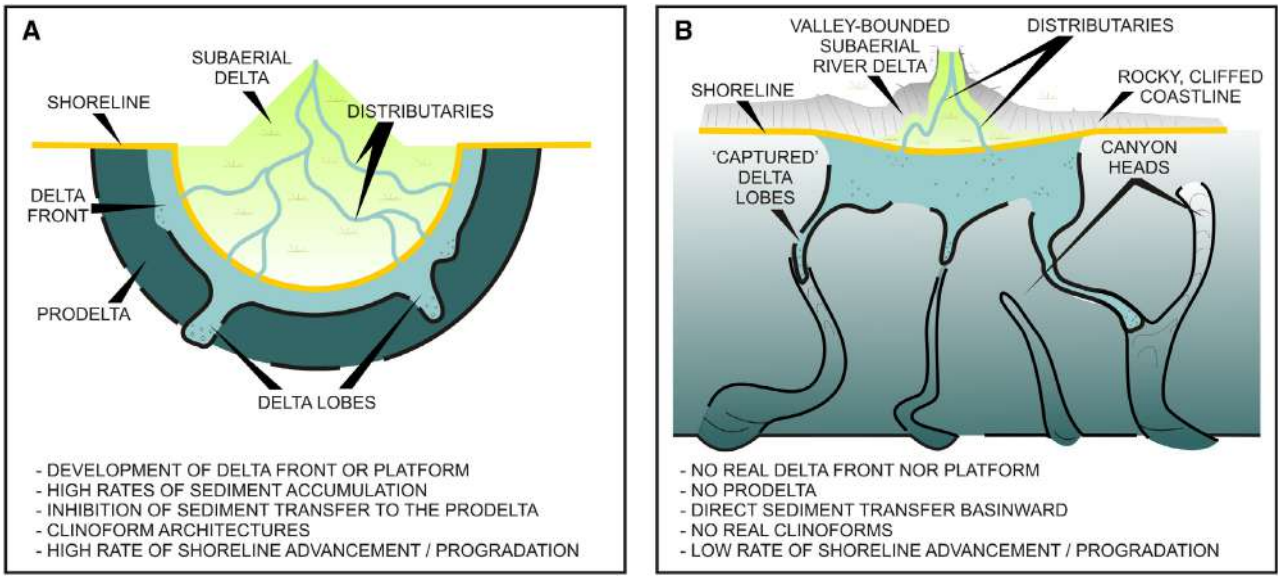

Fig. 22. (A) Simplified plan geometry typical of unconfined deltas. Subaqueous delta front and prodelta form radial axisymmetrical, laterally continuous sediment bands (modified, after Korus & Fielding, 2015). (B) Conceptual model proposed for canyon-captured deltas developing 'ephemeral' subaerial plains due to a lack of coastal space. Delta mouth-bars and lobes prograde directly into the canyons, preventing the radial development of subaqueous environments. This process would also reduce the probability to develop cross-sectional clinoform architectures, which are typical of deltas – example in (A).

of the various reconstructed branches that would reflect the original canyon geometry (Figs 18B and 21A). These deposits were successfully preserved by background processes of post-depositional reworking thanks to their protected position within the canyons.

This study indicates that: (i) no subaqueous delta-platform or delta-front environments developed, due to a lack of space (i.e. horizontal accommodation) for sediments to be radially distributed across the shallowest subaqueous portions of the system; (ii) prodelta fines were efficiently transferred farther basinward through the canyons by high-energy underflows, and were probably deposited as turbidites in the deepest, axial sectors of the strait; (iii) strata filling the canyons do not produce well-defined clinoform architectures; and (iv) due to this process of continuous subtraction of sediment from the coastline, the delta plain was generally characterized by a very low rate of advancement or progradation and was locally ephemeral or not developed at all, as observed along the present-day, high-relief coast of the region (Fig. 22B).

CONCLUSIONS

The analysis of the Lower Pleistocene succession presented in this work reconstructs the anatomy of a segment of the shallow-water margin of the ancient Messina Strait (southern Italy). Depositional architectures and facies characteristics, exposed in three dimensions, were key to outline the general features of a specific type of delta system, fed by valley-bounded rivers and entering canyon heads in the nearshore zone of tectonically-controlled, tide-influenced steep strait margins.

The observations herein show that the gradient of the sublittoral slope was a key prerequisite to promote processes of subaqueous slope incision and canyon retreating. These features are common along the sublittoral borders of the modern Messina Strait, where several studies have recently revealed analogous morphological and bathymetric features and their internal sedimentary dynamics. Outcrops documented in this study suggest the presence of a series of canyon entrances, which were possibly represented by multiple tributaries or branches oriented at different angles with respect to the palaeo-shoreline.

The initial phases of river delta progradation and consequent canyon infill occur through repeated episodes of fluvio-deltaic discharge attaining supercritical flow conditions in the proximal canyon segment. This early phase is recorded into a series of 5 to 10 m thick, amalgamated pebbly sandstone wedges preserved in Unit *A*, whose internal backsets indicate deposition under supercritical-flow conditions. The overlying Unit *B* records the subsequent burial of these canyons and their subaqueous interfluves with a series of migrating and laterally juxtaposed dune fields reflecting the tidal circulation of the strait.

- The subaqueous lateral confinement of hyperpycnal river-derived currents is another fundamental ingredient for the preservation of supercritical-flow structures with a wide range of scales. These deposits are in fact minimally reworked and eroded from background processes typical of nearshore zones, including waves and, in the specific case at hand, longshore-oriented tidal currents, thanks to the 'protection' and excess of accommodation offered by the canyon walls.
- Valley-bounded river deltas entering a shallow-water setting sculpted into a series of canyon heads develop a very unusual shape and configuration, which departs dramatically from standard models provided for subaqueous deltas for the following main reasons:
    - The process of sediment capture at canyon heads inhibits the formation of the fan-shaped, radially axisymmetrical plan-view geometry expected for unconfined delta fronts. On the contrary, deltas impinging canyon entrances in shallow waters promote lobe branching and the onset of supercritical-flow phenomena over other basinal processes more commonly recognized in stratigraphy, such as waves and tides.
    - Prodelta is virtually absent in these systems, as fines were mostly transferred farther basinward through the canyon fairways.
    - The lateral constraint exerted by the canyon confinement hampers the development of traditional clinoform architectures.
    - The continuous subtraction of sediment due to canyons in the nearshore area prevents delta plain advancement or progradation.

These elements thus suggest that the conventional attribution of deposits to subaqueous deltaic sub-environments (i.e. delta platforms,

fronts, slope and prodelta) cannot be applied in this specific setting and launch possible breakthroughs for future further investigations on this subject.

ACKNOWLEDGEMENTS

Authors thanks G. Postma, K. Lobo, D. Casalbore, C. Olariu and Associate Editor C. Fielding, whose critical reviews and insightful comments on an earlier version of this manuscript helped to sharpen the ideas presented in this study. SGL wants to express his personal gratitude to R.J. Steel, R.W. Dalrymple and D. Mellere, for the enthusiastic and very constructive discussions on the field. In particular, this latter firstly instilled to the first author the idea of the presence of an ancient canyon system in this part of the Messina Strait. DC thanks AkerBP, DNO, Neptune Energy and Spirit Energy for supporting the Phase I of the Joint Industry Project on Fault-controlled deposits and CSI research group. The Safari Project team is also acknowledged for LiDAR and drone acquisition of some of the sections documented in this study.

DATA AVAILABILITY STATEMENT

The data that support the findings of this study are available from the corresponding author upon reasonable request.

REFERENCES

Alexander, J. (2008) Bedforms in Froude-supercritical flow. In: *Marine and River Dune Dynamics* Conference Volume, pp. 1–5. Leeds University, Leeds.

Allen, J.R.L. (1980) Sand waves: a model of origin and internal structure. *Sed. Geol.*, **26**, 281–328.

Allen, J.R.L. (1982) *Sedimentary Structures: Their Character and Physical Basis*. Elsevier Science Publishers, Amsterdam, 592 pp.

Allen, P.A. and **Posamentier, H.W.** (1993) Sequence stratigraphy and facies model of an incised valley fill: the Gironde Estuary, France. *J. Sed. Res.*, **63**, 378–391.

Anastas, A., **Dalrymple, R.W.**, **James, N.P.** and **Nelson, C.S.** (1997) Genesis of subaqueous, cool-water carbonate dunes in an Oligo-Miocene seaway, North Island, New Zealand. *Sedimentology*, **44**, 869–891.

Androsov, A.A., **Kagan, B.A.**, **Romanenkov, D.A.** and **Voltzinger, N.E.** (2002) Numerical modelling of barotropic tidal dynamics in the strait of Messina. *Adv. Wat. Res.*, **25**, 401–415.

Ashley, G.M. (1990) Classification of large-scale subaqueous bedforms: a new look at an old problem. *J. Sed. Petrol.*, **60**, 160–172.

Ayranci, K., **Lintern, D.G.**, **Hill, P.R.** and **Dashtgard, S.E.** (2012) Tide-supported gravity flows on the upper delta front, Fraser River delta, Canada. *Mar. Geol.*, **326**, 166–170.

Barrier, P. (1984) Evolution tectono-sédimentaire pliocène et pléistocène du Détroit de Messine (Italie). Thesis Univ. Marseille, 270 pp.

Barrier, P. (1986) Évolution paléogéographique du Détroit de Messine au Pliocène et au Pléistocène. *G. Geol.*, **48**, 7–24.

Barrier, P. (1987a) Stratigraphie des dépôtsdépôts pliocènes et quaternaires du Détroit de Messine. Documents et Travaux d'Institut Geologique A. *De Lapparent, Paris*, **11**, 59–81.

Barrier, P. (1987b) La pérennité du Détroit de Messine au Quaternaire. Documents et Travaux d'Institut Geologique A. *De Lapparent, Paris*, **11**, 267–270.

Barrier, P., **Casale, V.**, **Costa, B.**, **Di Geronimo, I.**, **Oliveri, O.** and **Rosso, A.** (1987) La sezione plio-pleistocenica di Pavigliana (Reggio Calabria). *Boll. Soc. Pal. It.*, **25**, 107–144.

Barrier, P., **Gaudant, J.**, **Raisson, F.**, **Merle, D.** and **Toumarkine, M.** (1993) La lagune pléistocècene à Gobius Sp. du Monte Torre (Calabre méridionale, Italie): signification paléogéographique. *Riv. It. Pal. Strat.*, **99**, 127–140.

Baztan, J., **Berné, S.**, **Olivet, J.-L.**, **Rabineau, M.**, **Aslanian, D.**, **Gaudin, M.**, **Réhault, J.-P.** and **Canals, M.** (2005) Axial incision: the key to understand submarine canyon evolution (in the western Gulf of Lion). *Mar. Petrol. Geol.*, **22**, 805–826.

Bhattacharya, J.P. (2006) Deltas. In: *Facies Models Revisited* (Eds Posamentier, H.W. and Walker, R.G.). SEPM (Society for Sedimentary Geology). 237–292.

Bignami, F. and **Salusti, E.** (1990) Tidal currents and transient phenomena in the Strait of Messina: a review. In: *The Physical Oceanography of Sea Straits* (Ed. Pratt, L.J.), pp. 95–124. Kluwer Academic, Dordrecht.

Blair, T.C. and **McPherson, J.G.** (1999) Grain-size and textural classification of coarse sedimentary particles. *J. Sed. Res.*, **69**, 6–19.

Blikra, L.H. and **Nemec, W.** (1998) Postglacial colluvium in Western Norway: depositional processes, facies and palaeoclimatic record. *Sedimentology*, **45**, 909–959.

Cartigny, M.J.B., **Postma, G.**, **Van Den Berg, J.H.** and **Mastbergen, D.R.** (2011) A comparative study of sediment waves and cyclic steps based on geometries, internal structures and numerical modelling. *Mar. Geol.*, **280**, 40–56.

Cartigny, M.J.B., **Ventra, D.**, **Postma, G.** and **Van Den Berg, J.H.** (2014) Morphodynamics and sedimentary structures of bedforms under supercritical-flow conditions: new insights from flume experiments. *Sedimentology*, **61**, 712–748.

Casalbore, D., **Bosman, A.**, **Ridente, D.** and **Chiocci, F.L.** (2014) Coastal and submarine landslides in the tectonically-active Tyrrhenian Calabrian Margin (Southern Italy): examples and geohazard implications. In: *Submarine Mass Movements and Their Consequences. Advances in Natural and Technological Hazards Research* (Eds Krastel, S. et al.), vol. **37**, pp. 261–269.Springer, Cham.

Casalbore, D., **Bosman, A.**, **Casas, D.**, **Chiocci, F.**, **Martorelli, E.** and **Ridente, D.** (2019) Morphological variability of submarine mass movements in the tectonically–controlled Calabro-Tyrrhenian Continental Margin (Southern Italy). *Geosciences*, **9**, 43.

Casalbore, D., **Chiocci, F.L.**, **Scarascia Mugnozza, G.**, **Tommasi, P.** and **Sposato, A.** (2011) Flash-flood

hyperpycnal flows generating shallow-water landslides at Fiumara mouths in western Messina Strait (Italy). *Mar. Geoph. Res.*, **32**, 257–271.

Casalbore, D., **Martorelli, E.**, **Bosman, A.**, **Morelli, E.** and **Chiocci, F.L.** (2018) Failure dynamics of landslide scars on the lower continental slope of the Tyrrhenian Calabrian margin: insights from an integrated morpho-bathymetric and seismic analysis. *J. Geol. Soc. London Spec. Publ.*, **477**, 389–397.

Casalbore, D., **Ridente, D.**, **Bosman, A.** and **Chiocci, F.L.** (2017) Depositional and erosional bedforms in Late Pleistocene-Holocene pro-delta deposits of the Gulf of Patti (southern Tyrrhenian margin, Italy). *Mar. Geol.*, **385**, 216–227.

Cattaneo, A. and **Steel, R.J.** (2003) Transgressive deposits: a review of their variability. *Earth Sci. Rev.*, **62**, 187–228.

Chiarella, D. (2016) Angular and tangential toeset geometry in tidal cross strata: an additional feature of current-modulated deposits. In: *Contributions to Modern and Ancient Tidal Sedimentology* (Eds Tessier, B. and Reynaud, J.-Y.). Proceedings of the Tidalites 2012 Conference. IAS Special Publication, 185–195

Chiarella, D. and **Longhitano, S.G.** (2012) Distinguishing depositional environments in shallow-water mixed, bio-siliciclastic deposits on the basis of the degree of heterolithic segregation (Gelasian, southern Italy). *J. Sed. Res.*, **82**, 969–990.

Chiarella, D., **Longhitano, S.G.** and **Muto, F.** (2012) Sedimentary features of the Lower Pleistocene mixed siliciclastic–bioclastic tidal deposits of the Catanzaro Strait (Calabrian Arc, south Italy). *Rend. Online Soc. Geol.*, **21**, 919–920.

Chiarella, D., **Longhitano, S.G.** and **Tropeano, M.** (2017) Types of mixing and heterogeneities in siliciclastic-carbonate sediments. *Mar. Petrol. Geol.*, **88**, 617–627.

Chiarella, D., **Longhitano, S.G.** and **Muto, F.** (2020) Fault-controlled base-of-scarp deposits. *Bas. Res.*, **33**, 1056–1075.

Chiocci, F.L. and **Casalbore, D.** (2017) Unexpected fast rate of morphological evolution of geologically-active continental margins during Quaternary: examples from selected areas in the Italian seas. In: *Sedimentology in Italy: New Advances and Insights* (Eds Longhitano, S.G., Steel, R.J. and Pomar, L.). *Mar. Petrol. Geol., Special Issue*, **82**, 154–162.

Chiocci, F.L., **Catalano, R.D.**, **Geronimo, I.**, **Critelli, S.**, **Martorelli, E.**, **Barone, M.**, **Dominici, R.**, **Marchetti, M.**, **Rosso, A.**, **Valenti, V.** and **Zanini, A.** (2008) Note illustrative aree sommerse della carta geologica d'Italia alla scala 1:50 000, Foglio 601, 'Messina – Reggio di Calabria'. Agenzia per la protezione dell'ambiente e i servizi tecnici (APAT), Roma.

Cocco, E., **De Pippo, T.**, **De Lauro, M.** and **Monda, C.** (1988) Focus erosivi sul litorale metapontino (Golfo di Taranto). *Mem. Soc. Geol. Ital.*, **41**, 703–709.

Colella, A. and **D'Alessandro, A.** (1988) Sand waves, Echinocardium traces and their bathyal depositional setting (Monte Torre Palaeostrait, Plio-Pleistocene, southern Italy). *Sedimentology*, **35**, 219–237.

Collinson, J. and **Mountney, N.** (2006) *Sedimentary Structures*, 4th edn, pp. 340. Dunedin Academic Press Ltd, Edinburgh.

Cornard, P.H. and **Pickering, K.T.** (2019) Supercritical-flow deposits and their distribution in a submarine channel system, Middle Eocene, Ainsa Basin, Spanish Pyrenees. *J. Sed. Res.*, **89**, 576–597.

Corsini, S., **Franco, L.**, **Inghilesi, R.**, **Piscopia, R.**, **Panizzo, A.**, **Contini, P.**, **Milana, G.**, **Saltari, D.**, **De Girolamo, P.**, **Arseni, A.**, **Belloni, L.** and **Franco, C.** (2003) Italian Wave Atlas. APAT (ISPRA) Agenzia per la Protezione dell'Ambiente e per i Servizi Tecnici, Stampa IGER S.r.l. Roma, 123 pp.

Covault, J.A., **Kostic, S.**, **Paull, C.K.**, **Sylvester, Z.** and **Fildani, A.** (2017) Cyclic steps and related supercritical bedforms: building blocks of deep-water depositional systems, western North America. *Mar. Geol.*, **393**, 4–20.

Dalrymple, R.W. (1984) Morphology and internal structure of sand waves in the Bay of Fundy. *Sedimentology*, **31**, 365–382.

Dalrymple, R.W. (2010) Tidal depositional systems. In: *Facies Models 4* (Eds James, N.P. and Dalrymple, R.W.), pp. 199–208.Geological Association, Canada.

Dedkov, A.P. and **Mozzherin, V.I.** (1992) Erosion and sediment yield in mountain regions of the world. In: *Proceedings of the Chengdu Symposium, July 1992* (Eds Davies, E., Harsholt, T.R. and Walling, D.), IAHS Publication, **209**, 29–36.

Defant, A. (1940) Scilla e Cariddi e le correnti di marea nello Stretto di Messina. *Geof. Pur. Appl.*, **2**, 93–112.

Defant, A. (1961) *Physical Oceanography. 1, 2*. Pergamon Press, Oxford – London - New York – Paris, 1327.

Dewey, J.F., **Helman, M.L.**, **Turco, E.**, **Hutton, D.H.W.** and **Knott, S.D.** (1989) Kinematics of the Western Mediterranean. In: *Alpine Tectonics* (Eds Coward, M.P., Dietrich, D. and Parki, R.G.), *Geological Society of America. Spec. Publ.*, **45**, 265–284.

Di Celma, C., **Cantalamessa, G.**, **Landini, W.** and **Ragaini, L.** (2010) Stratigraphic evolution from shoreface to shelf-indenting channel depositional systems during transgression: insights from the lower Pliocene Súa Member of the basal Upper Onzole Formation, Borbón Basin, northwest Ecuador. *Sed Geol*, **223**, 162–179.

Di Stefano, A. and **Longhitano, S.G.** (2009) Tectonics and sedimentation of the Lower and Middle Pleistocene mixed bioclastic/siliciclastic sedimentary succession of the Ionian Peloritani Mts (NE Sicily, southern Italy): the onset of the Messina Strait opening. *Centr. Eur. J. Geosci.*, **1**, 33–62.

Doglioni, C. (1991) A proposal of kinematic modeling for W-dipping subductions - possible applications to the Tyrrhenian-Apennines system. *Terra Nova*, **3**, 423–434.

Doglioni, C., **Innocenti, F.** and **Mariotti, G.** (2001) Why Mt Etna? *Terra Nova*, **13**, 25–31.

Driscoll, N.W. and **Karner, G.D.** (1999) Three-dimensional quantitative modeling of clinoform development. *Mar. Geol.*, **154**, 383–398.

Dumas, B., **Gueremy, P.**, **Lhenaff, R.** and **Raffy, J.** (1982) Le soulèvement quaternaire de la Calabrie méridionale. *Revue de géologie dynamique et de géographie physique*, **23**, 27–40.

Fielding, C.R. (2006) Upper flow regime sheets, lenses and scour fills: extending the range of architectural elements for fluvial sediment bodies. *Papers in the Earth and Atmospheric Sciences*, **296**, 227–240.

Finetti, I.R., **Lentini, F.**, **Carbone, S.**, **Catalano, S.** and **Del Ben, A.** (1996) Il sistema Appennino Meridionale-Arco Calabro-Sicilia nel Mediterraneo centrale: studio geologico-geofisico. *Boll. Soc. Geol. Ital.*, **115**, 529–559.

Galloway, W.E. (1998) Siliciclastic slope and base-of-slope depositional systems: component facies, stratigraphic architecture, and classification. *AAPG Bull.*, **82**, 569–595.

Galloway, W.E. (2002) Paleogeographic setting and depositional architecture of a sand-dominated shelf

depositional system, Miocene Utsira Formation, North Sea Basin. *J. Sed. Res.*, **72**, 476–490.

Gamberi, F. (2020) Systems supplying sediment to canyon heads (SSSCHs) in the Tyrrhenian Sea: the past and the present as a key to understanding deep-sea stratigraphy. *Mar. Petrol. Geol.*, **119**, 104470.

Gamberi, F., **Breda, A.** and **Mellere, D.** (2017) Depositional canyon heads at the edge of narrow and tectonically steepened continental shelves: comparing geomorphic elements, processes and facies in modern and outcrop examples. *Mar. Petrol. Geol.*, **87**, 157–170.

Geleynse, N., **Storms, J.E.A.**, **Stive, M.J.F.**, **Jagers, H.R.A.** and **Walstra, D.-J.-R.** (2010) Modeling of a mixed-load fluvio-deltaic system. *Geoph. Res. Lett.*, **37**, L05402.

Geleynse, N., **Storms, J.E.A.**, **Walstra, D.-J.-R.**, **Jagers, H.R.A.**, **Wang, Z.B.** and **Stive, M.J.F.** (2011) Controls on river delta formation; insights from numerical modeling. *Earth Plan. Sci. Lett.*, **302**, 217–226.

Gelfenbaum, G., **Stevens, A.W.**, **Miller, I.**, **Warrick, J.A.**, **Ogston, A.S.** and **Eidam, E.** (2015) Large-scale dam removal on the Elwha River, Washington, USA: coastal geomorphic change. *Geomorphology*, **246**(1), 729–750.

Ghisetti, F. (1981a) Upper Pliocene-Pleistocene uplift rates as indicators of neotectonic pattern: an example from southern Calabria (Italy). *Z. Geomorph.*, **40**, 93–118.

Ghisetti, F. (1981b) L'evoluzione strutturale del bacino plio-pleistocenico di Reggio Calabria nel quadro geodinamico dell'Arco Calabro. *Boll. Soc. Geol. Ital.*, **100**, 433–466.

Ghisetti, F. (1984) Recent deformations and the seimogenic source in the Messina Strait (Southern Italy). *Tectonophysics*, **109**, 191–208.

Ghisetti, F. and **Vezzani, L.** (1982) The recent deformation mechanism of the Calabrian Arc. *Earth Environ. Sci.*, **3**, 197–206.

Ghisetti, F., **Vezzani, L.**, **Pezzino, A.** and **Atzori, P.** (1983) *Carta Geologica del Bordo Occidentale dell'Aspromonte*. SELCA, Firenze.

Goldhammer, R.K., **Dunn, P.A.** and **Hardie, L.A.** (1990) Depositional cycles, composite sea level changes, cycle stacking patterns and the hierarchy of stratigraphic forcing —examples from Alpine Triassic platform carbonates. *Geol. Soc. Am. Bull.*, **102**, 535–562.

Green, A.N., **Goff, J.A.** and **Uken, R.** (2007) Geomorphological evidence for upslope canyon-forming processes on the northern KwaZulu-Natal shelf, SW Indian Ocean, South Africa. *Geo-Mar. Lett.*, **27**, 399–409.

Hage, S., **Cartigny, M.J.B.**, **Clare, M.A.**, **Sumner, E.J.**, **Vendettuoli, D.**, **Hughes Clarke, J.E.**, **Hubbard, S.M.**, **Talling, P.J.**, **Lintern, D.G.**, **Stacey, C.D.**, **Englert, R.G.**, **Vardy, M.E.**, **Hunt, J.E.**, **Yokokawa, M.**, **Parsons, D.R.**, **Hizzett, J.L.**, **Azpiroz-Zabala, M.** and **Vellinga, A.J.** (2018) How to recognize crescentic bedforms formed by supercritical turbidity currents in the geologic record: insights from active submarine channels. *Geology*, **46**, 563–566.

Harms, J.C., **Southard, J.B.**, **Spearing, D.R.** and **Walker, R.G.** (1975) Depositional Environments as interpreted from Primary Sedimentary Structures and Stratification Sequences. *Soc. Sed. Geol. Short Course Lect. Notes*, **2**, 161.

Harms, J.C., **Southard, J.B.** and **Walker, R.G.** (1982) Structures and sequences in clastic rocks. *Soc. Sed. Geol. Short Course Lect. Notes*, **9**, 250.

Homewood, P. and **Allen, P.A.** (1981) Wave-, tide-, and current controlled sandbodies of Miocene Molasse, western Switzerland. *AAPG Bull.*, **65**, 2534–2545.

Hooke, J.M. (2019) Extreme sediment fluxes in a dryland flash flood. *Sci. Rep.*, **9**, 1686.

Hsiung, K.H. and **Saito, Y.** (2017) Sediment trapping in deltas of small mountainous rivers of southwestern Taiwan and its influence on East China Sea sedimentation. *Quat. Int.*, **455**, 30–44.

James, N.P., **Seibel, M.J.**, **Dalrymple, R.W.**, **Besson, D.** and **Parize, O.** (2014) Warm-temperate, marine, carbonate sedimentation in an Early Miocene, tide-influenced, incised valley; Provence, south-east France. *Sedimentology*, **61**, 497–534.

de Jonge, M.R., **Wortel, M.J.R.** and **Spakmankm, W.** (1994) Regional scale tectonic evolution and the seismic velocity structure of the lithosphere and upper mantle: the Mediterranean region. *J. Geoph. Res.*, **99**, 12091–12108.

Katz, T., **Ginat, H.**, **Eyal, G.**, **Steiner, Z.**, **Braun, Y.**, **Shalev, S.** and **Goodman-Tchernov, B.N.** (2015) Desert flash floods form hyperpycnal flows in the coral-rich Gulf of Aqaba, Red Sea. *Earth Planet. Sci. Let.*, **417**, 87–98.

Kazanci, N. and **Varol, B.** (1990) Development of a mass flow-dominated fan-delta complex and associated carbonate reefs within a transgressive Paleocene succession, central Anatolia, Turkey. *Sed. Geol.*, **68**, 261–278.

Keller, G.H. and **Richards, A.F.** (1967) Sediments of the Malacca Strait, Southeast Asia. *J. Sed. Petr.*, **37**, 102–127.

Komar, P.D. (1971) Hydraulic jumps in turbidity currents. *Geol. Soc. Am. Bull.*, **82**, 1477–1488.

Korup, K. (2012) Earth's portfolio of extreme sediment transport events. *Earth-Sci. Rev.*, **112**, 115–125.

Korus, J.T. and **Fielding, C.R.** (2015) Asymmetry in Holocene river deltas: patterns, controls, and stratigraphic effects. *Earth-Sci. Rev.*, **150**, 219–242.

Kostic, S., **Casalbore, D.**, **Chiocci, F.**, **Lang, J.** and **Winsemann, J.** (2019) Role of upper-flow-regime bedforms emplaced by sediment gravity flows in the evolution of deltas. *J. Mar. Sci. Eng.*, **7**, 5.

Kostic, S., **Parker, G.** and **Marr, J.G.** (2002) Role of turbidity currents in setting the foreset slope of clinoforms prograding into standing fresh water. *J. Sed. Res.*, **72**, 353–362.

Lamb, M.P., **McElroy, B.**, **Kopriva, B.**, **Shaw, J.** and **Mohrig, D.** (2010) Linking river-flood dynamics to hyperpycnal-plume deposits: experiments, theory, and geological implications. *GSA Bull.*, **122**, 1389–1400.

Lang, J. and **Winsemann, J.** (2013) Lateral and vertical facies relationships of bedforms deposited by aggrading supercritical flows: from cyclic steps to humpback dunes. *Sed. Geol.*, **296**, 36–54.

Langbein, W.B. and **Schumm, S.A.** (1958) Yield of sediment in relation to mean annual precipitation. *Trans. AGU*, **39**, 76–84.

Lentini, F., **Carbone, S.** and **Catalano, S.** (1994) Main structural domains of the central Mediterranean region and their tectonic evolution. *Boll. Geof. Teor. Appl.*, **36**, 103–125.

Lo Iacono, C., **Cartigny, M.**, **Zizzo, E.**, **Agate, M.** and **Sulli, A.** (2017) Potential Cyclic Steps in a Gully System of the Gulf of Palermo (Southern Tyrrhenian Sea). In: *Atlas of Bedforms in the Western Mediterranean* (Eds Guillén, J., Acosta, J., Chiocci, F.L. and Palanques, A.). Springer International Publishing. Ch. **36**, 235–240.

Lobo, F.J., **Goff, J.A.**, **Mendes, I.**, **Bárcenas, P.**, **Fernández-Salas, L.m.**, **Martín-Rosales, W.**, **Macías, J.** and **Díaz del Río, V.** (2015) Spatial variability of prodeltaic undulations on the Guadalfeo River prodelta: support to the genetic

interpretation as hyperpycnal flow deposits. *Mar. Geophys. Res.*, **36**, 309–333.

Lobo, F.J. and **Ridente, D.** (2014) Stratigraphic architecture and spatio-temporal variability of high-frequency (Milankovitch) depositional cycles on modern continental margins: an overview. *Mar. Geol.*, **352**, 215–247.

Longhitano, S.G. (2008) Sedimentary facies and sequence stratigraphy of coarse-grained Gilbert-type deltas within the Pliocene thrust-top Potenza Basin (Southern Apennines, Italy). *Sed. Geol.*, **210**, 87–110.

Longhitano, S.G. (2011) The record of tidal cycles in mixed silici–bioclastic deposits: examples from small Plio-Pleistocene peripheral basins of the microtidal Central Mediterranean Sea. *Sedimentology*, **58**, 691–719.

Longhitano, S.G. (2012) Microtidal straits: outcrop analogues from Calabria, south Italy. *Rend. On. Soc. Geol. It.*, **21**, 937–939.

Longhitano, S.G. (2013) A facies-based depositional model for ancient and modern, tectonically–confined tidal straits. *Terra Nova*, **25**, 446–452.

Longhitano, S.G. (2016) Sedimentology of supercritical-flow features preserved in the lower Pleistocene deltaic succession of the Messina Strait (Calabria, Italy). *Rend. Soc. Geol. Ital.*, **1**, 40, 608.

Longhitano, S.G. (2018a) Between Scylla and Charybdis (part 1): the sedimentary dynamics of the modern Messina Strait (central Mediterranean) as analogue to interpret the past. *Earth-Sci. Rev.*, **185**, 259–287.

Longhitano, S.G. (2018b) Between Scylla and Charybdis (part 2): the sedimentary dynamics of the ancient, Early Pleistocene Messina Strait (central Mediterranean) based on its modern analogue. *Earth-Sci. Rev.*, **179**, 248–286.

Longhitano, S.G., **Chiarella, D.**, **Di Stefano, A.**, **Messina, C.**, **Sabato, L.** and **Tropeano, M.** (2012b) Tidal signatures in Neogene to Quaternary mixed deposits of southern Italy straits and bays. In: *Modern and Ancient Tidal Depositional Systems: Perspectives, Models and Signatures* (Eds Longhitano, S.G., Mellere, D. and Ainsworth, B.), *Sed. Geol., Special Issue*, **279**, 74–96.

Longhitano, S.G., **Chiarella, D.** and **Muto, F.** (2014) Three-dimensional to two-dimensional cross-strata transition in the lower Pleistocene Catanzaro tidal strait transgressive succession (southern Italy). *Sedimentology*, **61**, 2136–2171.

Longhitano, S.G. and **Chiarella, D.** (2020) Tidal straits: basic criteria for recognizing ancient systems from the rock. In: *Regional Geology and Tectonics, Vol 1: Principles of Geologic Analysis* (Eds Scarselli, N., Adam, J., Chiarella, D., Roberts, D.G. and Bally, A.W.). Elsevier, Amsterdam, Netherlands, Ch. 15, 365–415.

Longhitano, S.G., **Chiarella, D.**, **Gugliotta, M.**, **Barrier, P.**, **Ventra, D.** and **Muto, F.** (2020) Tidal sedimentary dynamics of the Early Pleistocene Messina Strait (Calabria, southern Italy) based on its modern analogue. *Geol. Field Trips and Maps.*, **12**, 1–45.

Longhitano, S.G., **Mellere, D.**, **Steel, R.J.** and **Ainsworth, R.B.** (2012a) Tidal depositional systems in the rock record: A review and new insights. In: *Modern and Ancient Tidal Depositional Systems: Perspectives, Models and Signatures* (Eds Longhitano, S.G., Mellere, D. and Ainsworth, B.). *Sed. Geol., Special Issue*, **279**, 2–22.

Longhitano, S.G. and **Nemec, W.** (2005) Statistical analysis of bed-thickness variation in a Tortonian succession of biocalcarenitic tidal dunes, Amantea Basin, Calabria, southern Italy. *Sed. Geol.*, **179**, 195–224.

Longhitano, S.G., **Rossi, V.M.**, **Chiarella, D.** and **Mellere, D.** (2021) From marginal to axial tidal-strait facies in the early Pleistocene Siderno Strait. *Geol. Field Trips and Maps.*, in press

Longhitano, S.G. and **Steel, R.J.** (2016) Deflection of the progradational axis and asymmetry in tidal seaway and strait deltas: insights from two outcrop case studies. *J. Geol. Soc. London, Spec. Public.*, **444**, 141–172.

Lozano, C.J. and **Candela, J.** (1995) The M2 tide in the Mediterranean Sea: dynamic analysis and data assimilation. *Ocean. Acta*, **18**, 419–441.

Maier, K.L., **Johnson, S.Y.** and **Hart, P.** (2018) Controls on submarine canyon head evolution: Monterey Canyon, offshore central California. *Mar. Geol.*, **404**, 24–40.

Malinverno, A. and **Ryan, W.B.F.** (1986) Extension in the Tyrrhenian Sea and shortening in the Apennines as result of arc migration driven by sinking of the lithosphere. *Tectonics*, **5**, 227–245.

Massari, F. (1996) Upper-flow-regime stratification types on steep-face, coarse-grained, Gilbert-type progradational wedges (Pleistocene, Southern Italy). *J. Sed. Res.*, **66**, 364–375.

Massari, F. (2017) Supercritical-flow structures (backset-bedded sets and sediment waves) on high-gradient clinoform systems influenced by shallow-marine hydrodynamics. *Sed. Geol.*, **360**, 73–95.

McPherson, J.G., **Shanmugam, G.** and **Moiola, R.J.** (1987) Fan-deltas and braid deltas: varieties of coarse-grained deltas. *GSA Bull.*, **99**, 331–340.

Mercier, D., **Barrier, P.**, **Beaudoin, B.**, **Didier, S.**, **Montenat, J.L.** and **Salinas Zuniga, E.** (1987) Les facteurs hydrodynamiques dans la sédimentation plio-quaternaire du Détroit de Messine. Le Détroit de Messine (Italie). Evolution tectono-sedimentaire récente (Pliocène et Quaternaire) et environment actuel. *Doc. Trav. IGAL*, **11**, 171–183.

Millar, S.W.S. (2015) Colluvial Deposit. In: *Encyclopedia of Planetary Landforms* (Eds Hargitai, H. and Kereszturi, Á.). Springer, New York, NY.

Minter, N.J., **Buatois, L.A.** and **Mángano, M.G.** (2016) The conceptual and methodological tools of ichnology. In: *The Trace-Fossil Record of Major Evolutionary Events: Volume 1: Precambrian and Paleozoic* (Eds Mángano, M.G. and Buatois, L.A.), pp. 1–26.Springer, Netherlands, Dordrecht.

Mitchell, J.K., **Holdgate, G.R.**, **Wallace, M.W.** and **Gallagher, S.J.** (2007) Marine geology of the Quaternary Bass Canyon system, southeast Australia: a cool-water carbonate system. *Mar. Geol.*, **237**, 71–96.

Monaco, C., **Tortorici, L.**, **Nicolich, R.**, **Cernobori, L.** and **Costa, M.** (1996) From collisional to rifted basins: an example from the southern Calabrian arc (Italy). *Tectonophysics*, **266**, 233–249.

Montenat, C., **Barrier, P.** and **Di Geronimo, I.** (1987) The Strait of Messina, past and present: a review. *Documents et Travaux d'Institut Geologique A. De Lapparent, Paris*, **11**, 7–13.

Mosetti, F. (1992) Considerazioni sulla idrodinamica nello Stretto di Messina. *Rend. Fis. Acc. Lincei*, **9**, 269–281.

Mountjoy, J.J., **Barnes, P.M.** and **Pettinga, J.R.** (2009) Morphostructure and evolution of submarine canyons across an active margin: Cook Strait sector of the Hikurangi Margin, New Zealand. *Mar. Geol.*, **260**, 45–68.

Mulder, T. and **Alexander, J.** (2001) The physical character of subaqueous sedimentary density currents and their deposits. *Sedimentology*, **48**, 269–299.

Mutti, E., **Davoli, R.**, **Tinterri, R.** and **Zavala, C.** (1996) The importance of ancient fluvio-deltaic systems dominated by catastrophic flooding in tectonically active basins. *Mem. Sci. Geol. Univ. Padova*, **48**, 233–291.

Nemec, W. (1990) Aspects of sediment movement on steep delta slopes. In: *Coarse-Grained Deltas* (Eds Colella, A. and Prior, D.B.), *International Association of Sedimentologists. Spec. Publ.*, **10**, 29–74.

Nemec, W. (2009) What is a hyperconcentrated flow? Conference Paper of the IAS Annual Meeting, Alghero (Sardinia), 20-23 September 2009.

Nio, S.D. and **Yang, C.S.** (1991) Diagnostic attributes of clastic tidal deposits: a review. In: *Clastic Tidal Sedimentology* (Eds Smith, D.G., Reinson, G.E., Zaitlin, B.A. and Rahmani, R.A.). *Can. Soc. Petr. Geol. Mem.*, 3–28.

Olariu, C., **Steel, R.J.**, **Dalrymple, R.W.** and **Gingras, M.K.** (2012) Tidal dunes versus tidal bars: the sedimentological and architectural characteristics of compound dunes in a tidal seaway, the lower Baronia Sandstone (Lower Eocene), Ager Basin, Spain. *Sed. Geol.*, **279**, 134–155.

Ono, K. and **Plink-björklund, P.** (2018) Froude supercritical flow bedforms in deepwater slope channels? Field examples in conglomerates, sandstones and fine-grained deposits. *Sedimentology*, **65**, 639–669.

Ortega-Sánchez, M., **Lobo, F.J.**, **López-Ruiz, A.**, **Losada, M.A.** and **Fernández-Salas, L.M.** (2014) The influence of shelf-indenting canyons and infralittoral prograding wedges on coastal morphology: the Carchuna system in Southern Spain. *Mar. Geol.*, **347**, 107–122.

Orton, G.J. and **Reading, H.G.** (1993) Variability of deltaic processes in terms of sediment supply, with particular emphasis on grain size. *Sedimentology*, **40**, 475–512.

Patacca, E., **Sartori, R.** and **Scandone, P.** (1990) Tyrrhenian basin and Apenninic arcs: kinematic relation since Late Tortonian times. *Mem. Soc. Geol. Ital.*, **45**, 425–451.

Patton, P.C. (1988) Drainage basin morphometry and floods. In: *Flood Geomorphology* (Eds Baker, V.R. and Kochel, R.C.), pp. 51–64. John Wiley & Sons, New York.

Pierson, T.C. (2005) Hyperconcentrated flow: transitional process between water flow and debris flow. In: *Debris-flow Hazards and Related Phenomena* (Eds Jakob, M. and Hungr, O.), pp. 159–202. Springer, Berlin.

Postma, G. (1984) Mass-flow conglomerates in a submarine canyon: Abrioja fan-delta, Pliocene, southeast Spain. In: *Sedimentology of Gravels and Conglomerates* (Eds. Koster, E.H. and Steel, R.J.). *Can. Soc. Petr. Geol. Memoir*, **10**, 237–258.

Postma, G. (1995) Sea level changes and the architectural response on coarse grained delta architecture. In: *Fan Deltas: Depositional Styles and Controls* (Eds Chough, S.K. and Orton, G.J.). *Sed. Geol.*, **98**, 3–12.

Postma, G., **Hoyal, D.C.**, **Abreu, V.**, **Cartigny, M.J.B.**, **Demko, T.**, **Fedele, J.J.**, **Kleverlaan, K.** and **Pederson, K.H.** (2016) Morphodynamics of supercritical turbidity currents in the channel-lobe transition zone. In: *Submarine Mass Movements and Their Consequences* (Eds. Lamarche, G., Mountjoy, J., Bull, S., Hubble, T., Krastel, S., Lane, E., Micallef, A., Mueller, L., Pecher, I. and Woelz, S.), Advances in Natural and Technological Hazards Series, vol. **41**, pp. 469–478. Springer Science, Dordrecht.

Postma, G., **Lang, J.**, **Hoyal, D.C.**, **Fedele, J.J.**, **Demko, T.**, **Abreu, V.** and **Pederson, K.H.** (2021) Reconstruction of bedform dynamics controlled by supercritical flow in the channel–lobe transition zone of a deep-water delta (Sant Llorenç del Munt, north-east Spain, Eocene). *Sedimentology*, **68**, 1674–1697.

Postma, G. and **Roep, T.B.** (1985) Resedimented conglomerates in the bottomsets of Gilbert-type gravel deltas. *J. Sediment. Petrol.*, **55**, 874–885.

Ridente, D. (2016) Releasing the sequence stratigraphy paradigm. Overview and perspectives. *J. Geol. Soc. London*, **173**, 845–853.

Rossi, V.M., **Longhitano, S.G.**, **Mellere, D.**, **Dalrymple, R.W.**, **Steel, R.J.**, **Chiarella, D.** and **Olariu, C.** (2017) Interplay of tidal and fluvial processes in an early Pleistocene, delta-fed, strait margin (Calabria, Southern Italy). *Mar. Petrol. Geol.*, **87**, 14–30.

Russell, H.A.J. and **Arnott, R.W.C.** (2003) Hydraulic-jump and hyperconcentrated-flow deposits of a glacigenic subaqueous fan: Oak Ridge Moraine, southern Ontario, Canada. *J. Sed. Res.*, **73**, 887–905.

Santoro, V.C., **Amore, E.**, **Cavallaro, L.** and **De Lauro, M.** (2004) Evolution of sand waves in the Messina Strait, Italy. *Ocean Dyn.*, **54**, 392–398.

Selli, R., **Colantoni, P.**, **Fabbri, A.**, **Rossi, S.**, **Borsetti, A.M.** and **Galignani, P.** (1978) Marine geological investigation on the Messina Straitss and its approaches. *Giorn. Geol.*, **2**, 1–22.

Sequeiros, O.E. (2012) Estimating turbidity current conditions from channel morphology: a Froude number approach. *J. Geophys. Res.*, **117**, C04003. https://doi.org/10.1029/2011JC007201

Seybold, H., **Andrade, J.S.** and **Herrmann, H.J.** (2007) Modeling river delta formation. *Proc. Natl. Acad. Sci.*, **104**, 16804–16809.

Shanmugam, G. (2018) The hyperpycnite problem. *J. Palaeogeogr.*, **7**, 1–42.

Shepard, F.P. (1981) Submarine canyons: multiple causes and long-time persistence. *AAPG Bull.*, **65**, 1062–1077.

Silva, T.A., **Girardclos, S.**, **Stutenbecker, L.**, **Bakker, M.**, **Costa, A.**, **Schlunegger, F.**, **Lane, S.N.**, **Molnar, P.** and **Loizeau, J.-L.** (2019) The sediment budget and dynamics of a delta-canyon-lobe system over the Anthropocene timescale: The Rhone River delta, Lake Geneva (Switzerland/France). *Sedimentology*, **66**, 838–858.

Sohn, Y.K., **Choe, M.Y.** and **Jo, H.R.** (2002) Transformation from debrisflow to hyperconcentrated flow in a submarine channel (the Cretaceous Cerro Toto Formation, southern Chile). *Terra Nova*, **14**, 405–415.

Sorriso-Valvo, M. (2008) Natural hazards and natural heritage – common origins and interference with cultural heritage. *Geogr. Fis. Dinam. Quat.*, **31**, 231–237.

Sorriso-Valvo, M. and **Terranova, O.** (2006) The Calabrian fiumara streams. *Z. Geomorphol.*, **143**, 109–125.

Southard, J.B. (1991) Experimental determination of bed-form stability. *Ann. Rev. Earth Plan. Sci.*, **19**, 423–455.

Stacey, C.D., **Hill, P.R.**, **Talling, P.J.**, **Enkin, R.J.**, **Hughes Clarke, J.** and **Lintern, D.G.** (2019) How turbidity current frequency and character varies down a fjord-delta system: combining direct monitoring, deposits and seismic data. *Sedimentology*, **66**, 1–31.

Swenson, J.B., **Paola, C.**, **Pratson, L.**, **Voller, V.R.** and **Murray, A.B.** (2005) Fluvial and marine controls on combined subaerial and subaqueous delta progradation: morphodynamic modeling of compound-clinoform development. *J. Geophys. Res.*, **110**, F02013.

Swift, D.J.P., **Hudelson, P.M.**, **Brenner, R.L.** and **Thompson, P.** (1987) Shelf construction in a foreland basin: stormbeds, shelf sand bodies, and shelf-slope depositional

sequences in the Upper Cretaceous Mesaverde Group, Book Cliffs, Utah. *Sedimentology*, **34**, 423–457.

Taylor, A.M. and **Goldring, R.** (1993) Description and analysis of bioturbation and ichnofabric. *J. Geol. Soc.*, **150**, 141–148.

Telesca, D., **Longhitano, S.G.**, **Pistis, M.**, **Pascucci, V.**, **Tropeano, M.** and **Sabato, L.** (2020) Sedimentology of a transgressive middle-upper Miocene succession filling a tectonically confined, current dominated seaway (the Logudoro Basin, northern Sardinia, Italy). *Sed. Geol.*, **400**, 105626.

Tinterri, R. (2011) Combined flow sedimentary structures and the genetic link between sigmoidal- and hummocky-cross stratification. *GeoActa*, **10**, 43–85.

Tubau, X., **Paull, C.K.**, **Lastras, G.**, **Caress, D.W.**, **Canals, M.**, **Lundsten, E.**, **Anderson, K.**, **Gwiazda, R.** and **Amblas, D.** (2015) Submarine canyons of Santa Monica Bay, southern California: variability in morphology and sedimentary process. *Mar. Geol.*, **365**, 61–79.

Urgeles, R., **Cattaneo, A.**, **Puig, P.**, **Liquete, C.**, **De Mol, B.**, **Amblás, D.**, **Sultan, N.** and **Trincardi, F.** (2011) A review of undulated sediment features on Mediterranean prodeltas: distinguishing sediment transport structures from sediment deformation. *Mar. Geophys. Res.*, **32**, 49–69.

Van Yperen, A.E., **Poyatos-Moré, M.**, **Holbrook, J.M.** and **Midtkandal, I.** (2020) Internal mouth-bar variability and preservation of subordinate coastal processes in low-accommodation proximal deltaic settings (Cretaceous Dakota Group, New Mexico, USA). *Dep. Rec.*, **6**, 431–458.

Ventra, D., **Cartigny, M.J.B.**, **Bijkerk, J.F.** and **Acikalin, S.** (2015) Supercritical-flow structures on a Late Carboniferous delta front: sedimentologic and paleoclimatic significance. *Geology*, **43**, 731–734.

Ventra, D. and **Clarke, L.E.** (2018) Geology and geomorphology of alluvial fans: current progress and research perspectives. In: *Geology and Geomorphology of Alluvial and Fluvial Fans: Terrestrial and Planetary Perspectives* (Eds Ventra, D. and Clarke, L.E.). *Geol. Soc. London Spec. Publ.*, **440**, 1–21.

Vercelli, F. (1925) Il regime delle correnti e delle maree nello Stretto di Messina. *Commissione Internazionale del Mediterraneo*, Campagne della R. Nave Marsigli negli anni 1922 e 1923, 209 p.

Visser, M.J. (1980) Neap-spring cycles reflected in Holocene subtidal large-scale bedform deposits: a preliminary note. *Geology*, **8**, 543–546.

Walker, R.G. (1984) General introduction: facies, facies sequences and facies models. In: *Facies Models*, 2nd edn (Ed. Walker, R.G.). *Geoscience Canada Reprint Series*, **1**, 1–9.

Wang, H., **Bi, N.**, **Wang, Y.**, **Saito, Y.** and **Yang, Z.** (2010) Tide-modulated hyperpycnal flows off the Huanghe (Yellow River) Mouth, China. *Earth Surf. Proc. Land.*, **35**, 1315–1329.

Warrick, J.A. and **Milliman, J.D.** (2003) Hyperpycnal sediment discharge from semiarid southern California rivers: implications for coastal sediment budgets. *Geology*, **31**, 781–784.

Warrick, J.A., **Xu, J.P.**, **Noble, M.** and **Lee, H.J.** (2008) Rapid formation of hyperpycnal sediment gravity currents offshore of a semi-arid California river. *Cont. Shelf Res.*, **28**, 991–1009.

West, L.M., **Perillo, M.M.**, **Olariu, C.** and **Steel, R.J.** (2019) Multi-event organization of deep-water sediments into bedforms: long-lived, large-scale antidunes preserved in deep-water slopes. *Geology*, **47**, 391–394.

Westaway, R. (1993) Quaternary uplift of southern Italy. *J. Geophys. Res.*, **98**, 21741–21772.

Wynn, R.B., **Piper, D.J.W.** and **Gee, M.J.R.** (2002) Generation and migration of coarse-grained sediment waves in turbidity current channels and channel-lobe transition zones. *Mar. Geol.*, **192**, 59–78.

Yang, T., **Cao, Y.** and **Wang, Y.** (2017) A new discovery of the early cretaceous supercritical hyperpycnal flow deposits on Lingshan island, East China. *Acta Geol. Sinica*, **91**, 749–750.

Yokokawa, M., **Okuno, K.**, **Nakamura, A.**, **Muto, T.**, **Miyata, T.**, **Naruse, H.** and **Parker, G.** (2009) Aggradational cyclic steps: sedimentary structures found in flume experiments. 33rd IAHS Congress, Proceedings, pp. 5547–5554.

Yoshikawa, S. and **Nemoto, K.** (2010) Seasonal variations of sediment transport to a canyon and coastal erosion along the Shimizu coast, Suruga Bay, Japan. *Mar. Geol.*, **271**, 165–176.

Zaitlin, B.A., **Dalrymple, R.W.** and **Boyd, R.** (1994) The stratigraphic organization of incised-valley systems associated with relative sea-level change. In: *Incised-Valley Systems: Origin and Sedimentary Sequences* (Eds Dalrymple, R.W., Boyd, R. and Zaitlin, B.A.). *SEPM, Special Publication*, **51**, 45–60.

Manuscript received 14 August 2020; revision accepted 16 February 2021